



OPEN

Photovoltaic solar energy prediction using the seasonal-trend decomposition layer and ASOA optimized LSTM neural network model

Venkatachalam Mohanasundaram¹✉ & Balamurugan Rangaswamy²

As the global energy demand continues to produce, photovoltaic (PV) solar energy has emerged as a key Renewable Energy Source (RES) due to its sustainability and potential to reduce dependence on fossil fuels. However, accurate forecasting of Solar Energy (SE) output remains a significant challenge due to the inherent variability and intermittency of solar irradiance (SI), which is affected by factors such as weather conditions, geographic location, and seasonal patterns. Reliable prediction models are crucial for optimizing energy management, ensuring grid stability, and minimizing operational costs. To address these challenges, this research introduces an innovative method that integrates Robust Seasonal-Trend Decomposition (RSTL) with an Adaptive Seagull Optimisation Algorithm (ASOA)-optimized Long Short-Term Memory (LSTM) neural network. Using RSTL to differentiate between time series data into development, seasonal in nature, and residual factors, this methodology addresses SI's unpredictable nature and intermittent operation and provides the basis for accurate predictions. ASOA improves LSTM features by constantly finding and exploiting resources and adopting motivation from seagulls' collecting and migration behaviours. Parameter standardization employing ASOA, the RSTL decomposition approach, and the conceptual model of LSTM networks are all presented in this research work. The proposed method has been contrasted with conventional methods by applying a testing environment incorporating essential Meteorological Factors (MF) and historical SE datasets. The study of performance measurements (RMSE, MAE, and R²) demonstrates significant improvements in the accuracy of predictions. The research results highlight significant implications regarding subsequent studies and real-world uses in SE prediction, accentuating the positive impacts of incorporating accurate data decomposition and adaptive optimized performance.

Keywords Photovoltaic solar energy, Energy prediction model, Long short-term memory, Adaptive seagull optimisation, Accuracy

Photovoltaic (PV)-Solar Energy (SE) is an evolving and starting Renewable Energy Source (RES) that provides numerous advantages over traditional petroleum and natural gas¹. The development of accurate prediction models for SE generation is a prerequisite for the development of the global adoption of SE systems². Cost optimization, sustainable grid operations, and reliable energy management are every prospective result of well-balanced demand and supply predictions³. Solar Irradiance (SI) is impacted by weather conditions, geographical location, and seasons of the year, making it challenging to generate accurate SE predictions considering its vital unpredictability and inconsistency⁴. Various statistical models have traditionally been employed to predict SE output, including Autoregressive Integrated Moving Average (ARIMA), Holt-Winters exponential smoothing, and linear regression models⁵. These approaches are designed to capture patterns such as trends and seasonality in SI data⁶. However, these traditional models often struggle with SE data's inherent variability and complexity⁷. SI is influenced by multiple non-linear factors such as weather conditions, geographical location, and seasonal variations, making it difficult for traditional statistical models to provide accurate predictions, mainly when

¹Department of Electrical and Electronics Engineering, Kongu Engineering College, Perundurai, Tamil Nadu 638060, India. ²Department of Electrical and Electronics Engineering, K.S.Rangasamy College of Technology, Tiruchengode, Tamil Nadu 637215, India. ✉email: chalam203@gmail.com

dealing with longer-term or irregular data. These methods also fail when managing massive volumes of datasets or handling the noise and outliers typically found in SE data⁸.

Combining *state-of-the-art* Machine Learning (ML) techniques with reliable data deconstruction techniques has significantly solved these challenges. Long Short-Term Memory (LSTM) networks, another Recurrent Neural Network (RNN) type, are growing increasingly common among those techniques because they can analyze and accurately predict time-series data. LSTM is the method to proceed with SE prediction because of how effectively it records patterns and correlations over time⁹. However, optimizing LSTM features remains challenging, and it frequently results in unacceptable performance because of drawbacks like delayed convergence and the threat of falling lost in local optima¹⁰.

As discussed above, the problem of accurately predicting PV-SE output arises from the inherent variability of SI, influenced by dynamic factors like weather, geographical location, and seasonal shifts. Traditional models such as ARIMA and Holt-Winters struggle to handle solar energy data's complexity and non-linear nature, especially when dealing with irregularities and noise. While LSTM networks provide improved performance in capturing long-term dependencies, they face challenges like slow convergence, local minima traps, and difficulties managing noise and abrupt data shifts. This research aims to develop a more reliable and accurate prediction model for PV-SE by addressing both the limitations of traditional models and the optimization challenges faced by LSTM networks. The proposed solution integrates an Adaptive Seagull Optimisation Algorithm (ASOA)-optimized LSTM with Robust Seasonal-Trend Decomposition (RSTL), which decomposes the time-series data into trend, seasonal, and residual components. This combination seeks to improve the LSTM's predictive performance by efficiently managing data complexity and optimizing its parameters dynamically.

This paper introduces a detailed structure for PV-SE prediction using an LSTM- Neural Network (NN) model optimized for ASOA and relying on RSTL decomposition. The primary objective of the current research proposal is to improve PV-SE prediction accuracy by integrating an ASOA-optimized LSTM-NN along with the RSTL. By partitioning time series data into trend, seasonal in nature, and residual factors, the RSTL rapidly minimizes background noise, unexpected changes, and outliers. Prediction accuracy is enhanced primarily by this substantial decomposition, resulting in a more robust data repository for the LSTM. The ASOA optimizes in an approach that balances exploration and exploitation, using motivation from seagulls' foraging and migration behaviours. Adding an adaptive modulation factor that shifts depending on algorithm efficiency, ASOA generates a more adaptable and dynamic optimization method, improving the parameter selection and the model's overall performance. This encompassing method applies Adaptive Optimization (AO) and accurate data decomposition to address the complex nature and variations in SE data, consequently attempting to generate reliable SE predictions.

The main contributions of this work are as follows:

1. *Development of a Hybrid Prediction Model* A novel hybrid model is introduced, integrating RSTL with AS-OA-optimized LSTM to improve the accuracy and reliability of PV-SE predictions.
2. *Application of RSTL* The RSTL method is used to decompose time-series data into trend, seasonal, and residual components, which enhances data processing by reducing noise and managing outliers effectively.
3. *Dynamic Optimization with Adaptive Seagull Optimization Algorithm (ASOA)* ASOA is applied to optimize LSTM parameters dynamically, balancing exploration and exploitation to avoid issues like slow convergence and local minima traps commonly associated with LSTM models.
4. *Enhanced Prediction Accuracy* The proposed model addresses the limitations of traditional statistical and ML models by combining robust data decomposition with adaptive optimization, resulting in significant improvements in predictive accuracy for PV-SE output.
5. *Evaluation on Real-World Dataset* The model is tested on a comprehensive PV-SE generation and MF dataset, demonstrating its effectiveness and potential applicability in real-world scenarios.

The paper is organized as follows: Section "[Literature review](#)" presents the literature review, Section "[Overview of techniques](#)" presents the techniques employed, Section "[Methodology](#)" presents the methodology proposed, Section "[Experimental analysis](#)" presents the experiment analysis, and Section "[Conclusion and future work](#)" conclusion and future work of study.

Literature review

Cornaro et al.¹¹ used statistical models to find correlations between meteorological history data and hourly SI, establishing an early foundation for understanding SE patterns through historical data. Sbrana (2014)¹² expanded on these statistical methods by developing the Exponentially Weighted Moving Average (EWMA) approach, which further improved the ability to capture short-term trends in time-series data. However, these methods were still limited in addressing seasonality, which led to the introduction of the Holt-Winters approach^{13,14}. This method provided a more effective method to manage trends and seasonality in time-series data¹⁵.

Building on these techniques, researchers such as¹⁶ employed ARMA to analyze stationary and sequential features in SI time series, which enabled more precise pattern recognition. AlKandari and Ahmad¹⁷ further determined that ARMA was effective for static data analysis, but their reliance on stationary data posed limitations when handling more dynamic, non-linear patterns in SI, which became a key challenge for future models.

Nevertheless, the approach relies on static time series data, which is a big drawback. This limitation arises because models like ARMA and ARIMA assume stationarity, meaning the statistical properties of the time series remain constant over time. However, SI data is inherently non-static, influenced by dynamic factors such as weather conditions, geographical location, and seasonal changes. These models struggle to capture non-stationary behavior, making them less effective for accurate SE predictions, particularly in the face of long-term

trends or unexpected shifts. They used ARIMA to predict the SI field and summarised the coupling technique between AR and MA and how it handles non-static data. Haider et al.¹⁸ used the ARIMA method to anticipate SI and compared the findings to an ANN model's findings. A different approach employed a technique known as an ensemble to fusion statistical models with other models, resulting in a hybrid that exploited the strengths of all the member models. Typically, these compound models outperform traditional ANN or statistical models.

Statistical approaches, including SARIMAX and Prophet, were used by¹⁹ in tandem with ML algorithms such as LSTM, a modified version of RNN, CNN, and ANN. The prediction approaches in this research were selected based on their ability to work with time series data, and this work tested multiple model configurations that are appropriate for the test dataset. Every model's performance is evaluated using a variation of error metrics, including Coefficient of Determination (R^2), Mean Absolute Error (MAE), Mean Square Error (MSE), and Root Mean Square Error (RMSE). This study's primary contribution is the collection of data to conduct research towards the goal of RE's future. Moreover, based on the test methods used on the data in this study, it is intuitively clear that ANN, CNN, and LSTM perform best for short-term predictions, whereas SARIMAX and Prophet are the most efficient for long-term prediction.

Building on this concept²⁰, propose a hybrid model that integrates ML with Theta statistical methods to improve the accuracy of future SE generation from Renewable Energy (RE) facilities. The ML models contain LSTM, Gate Recurrent Unit (GRU), AutoEncoder LSTM (Auto-LSTM), and a new Auto-GRU. To improve the accuracy of the proposed Machine Learning and Statistical Hybrid Model (ML-SHM), they use two diversity methods: structural diversity and data diversity. This study uses four combined methods to integrate the ensemble members' predictions in the recommended ML-SHM: basic averaging, weighted averaging using linear and non-linear approaches, and variance-based combination applying the inverse method. The proposed ML-SHM was validated using two real-time series datasets: Shagara in Kuwait and Cocoa in the United States of America. The results reveal that the recommended ML-SHM, which used all combination methods, outperformed the predictions of typical individual models. The findings show that a hybrid model, which combines ML and statistical methods, outperforms one that integrates ML without statistical approaches. This work demonstrates the benefit of combining traditional statistical methods with ML, aligning to integrate robust data decomposition techniques with advanced ML models to enhance prediction accuracy, which is also central to the proposed approach.

For prediction SE generation one day in advance, Gundu and Simon²¹ presented a simplified ML approach based on the LSTM algorithm. The suggested simple LSTM outperforms the MLP model based on ML procedures such as data processing, model fitting, cross-validation, metrics evaluation, and hyperparameter tweaking. Furthermore, the LSTM's prediction can accurately capture intra-hour ramping under a variation of MF. The average RMSE is 0.512, which is highly encouraging and suggests that the deployed approaches are best suited for short-term SE prediction. Building on this, Beigi et al.²² designed an LSTM prediction model. Statistical analysis of multiple network models generates the optimal network topology for effective SE and temperature predictions. An II-Layer LSTM framework, with 10 nodes in Layer I and 20 nodes in Layer II, has been demonstrated to be the most efficient model for predicting SE and temperature data using statistical methods. In contrast to temperature data, which generates 0.014 MAPE and 1.0423 RMSE, solar data indicates that the advised LSTM model generates 0.2478 MAPE and 6.7207 RMSE. When compared with numerous frequently employed network algorithms in the technical literature, the model exhibited higher prediction accuracy.

Continuing with this exploration of LSTM's capabilities²³, Deep Learning (DL) techniques were used to discuss a method for estimating short-term generated SE of PV power plants. As mentioned earlier, an LSTM-based DL is assessed for its capacity to predict SE data to achieve those. The performance of the LSTM was evaluated and compared to the Multi-layer Perceptron (MLP) using the following metrics: MAE, MAPE, RMSE, and R^2 . The best performance of the LSTM for each day grouping is demonstrated in the prediction results. As a result, it delivers reliable information that will allow PV-SE power plants to run more efficiently in the future. The binomial formed by the concepts of DL and energy efficiency appears to have a promising future, particularly in terms of energy sustainability, decarbonization, and the digitalization of the electrical industry.

Next, Kumar and Sam²⁴ intended to assess the success rate of the Artificial Neural Network (ANN) approach to predicting and calculating SE outputs from Photovoltaic Power Systems (PVPS) using meteorological data. The review of the literature drove the selection of input variables for the RNN, which, in consequence, impacted the electrical power generation in the PVPS. This study investigated the RNN's capacity for predicting the PVPS's electricity generation for days that had not been stored in the training database after training the entire network. With an RMSE of 0.0248 and an average actual result energy of 0.538 MJ for any particular sample day, the trained RNN's performance evaluation generated a regression value of 0.97774 for the test results. Validation results showed that the trained RNN had good prediction accuracy, and different metrics used for evaluating the network's performance contained RMSE, an error histogram, and regression graphs developed in MATLAB.

To address the limitations of using only ML or DL techniques, Wen et al.²⁵ introduced a hybrid framework. The research study used two types of decomposition techniques: time series decomposition into the time and frequency domains via Seasonal-Trend Decomposition Layer (STL) and Discrete Wavelet Transformation (DWT), respectively, to achieve its goal of analyzing and quantifying SI predictions. The deconstructed detail and approximation components are predicted using an LSTM. The final Global Horizontal Irradiance (GHI) prediction is attained by integrating these components with the help of inverse wavelet transform. Using hourly data from January 2017 to June 2019, the suggested methodology has been shown using the Indian Meteorological Department (IMD) of Jodhpur, Rajasthan. The accuracy of predictions derived from the suggested model has been compared with that of different models. In the beginning, LSTM; next, hybrid STL + LSTM; third, in that order Bi-LSTM; and fourth, Persistence Model all performed poorly outperformed by the indicated hybrid STL + WT + LSTM.

Further, to represent the complex patterns and dynamics of PV-SE data, a combination model incorporating the best features of the STL, LSTM, SDE, and MA approaches was put forward by²⁶. The framework has been refined by focusing more on accurate predictions using the enhanced Whales Optimisation Algorithm (IWOA). Drawing inspiration from the collaborative foraging methods humpback whales perform, IWOA is an innovative optimization algorithm. IWOA further improves model accuracy by improving search features and convergence rates^{27,28}. The envisioned hybrid STL-LSTM-SDE-MA model, optimized with IWOA, has been verified using real-time SE data. The model outperformed different conventional prediction approaches in terms of reliability and accuracy. This optimized hybrid model is a *state-of-the-art* methodological tool for PV-SE prediction and is vital for a more resilient and viable future^{29,30}.

Overview of techniques

LSTM model

Unlike RNN, the state of an LSTM is regulated by an Input Gate (IG), a Forget Gate (FG), and an Output Gate (OG). The FG is specifically intended to discard memory cell information. The FG mechanism receives the OG value of the above layer and the current time input value. Its retention of the unit state at a previous time is then determined by calculating a probability value using the sigma function^{31–34}. The IG is also in charge of updating the cell status with fresh data. In greater detail, the output value of the function impacts the probability of a state update, and the function generates a new input value³⁵. Based on the current internal state, the OG determines how to regulate the output of the external state.

The process can be represented by Eq. (1) to Eq. (6).

$$f_t = \sigma(W_f x_t + U_f h_{t-1} + b_f) \quad (1)$$

$$i_t = \sigma(W_i x_t + U_i h_{t-1} + b_i) \quad (2)$$

$$o_t = \sigma(W_o x_t + U_o h_{t-1} + b_o) \quad (3)$$

$$\tilde{C}_t = \tanh(W_c x_t + U_c h_{t-1} + b_c) \quad (4)$$

$$C_t = f_t \odot C_{t-1} + i_t \odot \tilde{C}_t \quad (5)$$

$$h_t = o_t \odot \tanh(C_t) \quad (6)$$

where the input vector's weight matrices are represented by 'a', 'b', and 'c'. 'd', 'e', and 'f' represent the weight matrices from the final state to the hidden state. There is a use of bias weights 'g', 'h', and 'l'. The symbol 'm' indicates the multiplication of the matrix. 'n' is an input vector at that time³⁶. 'O' represents the output vector at a time. 'p' represents the cell status at the time. Figure 1 shows the LSTM cell.

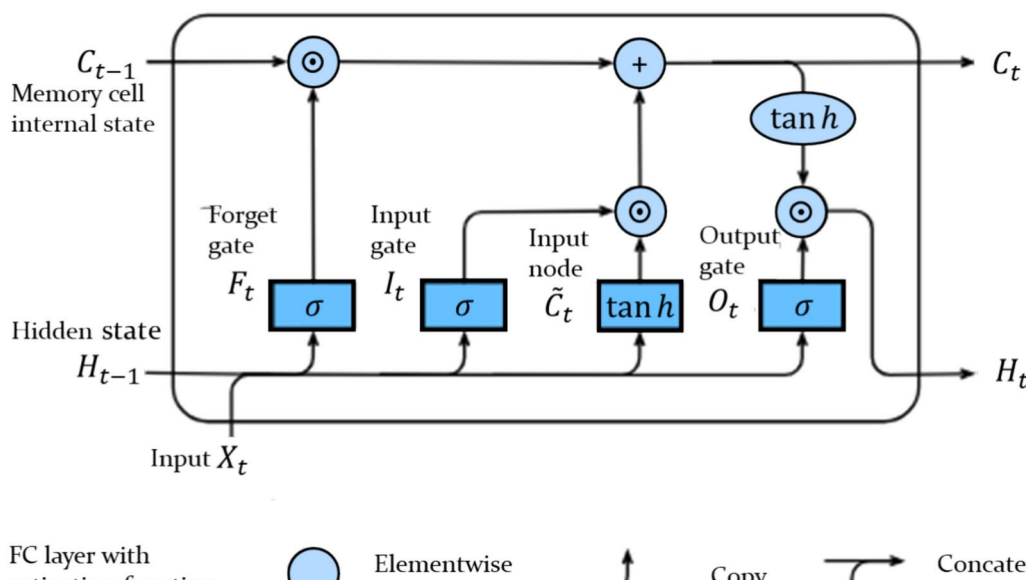


Fig. 1. The LSTM model.

Robust STL

To successfully analyze time series data with trend, seasonality, and residuals, we use the RSTL decomposition in this proposed SE prediction model³⁷. The description of the RSTL can be as follows: Eq. (7).

$$y_t = \tau_t + s_t + r_t, t = 1, 2, \dots, N \quad (7)$$

where the observed SE output data is represented by y_t , the trend component that captures long-term changes in SE generation is represented by τ_t , s_t mirrors seasonal swings in SE generation, and r_t comprises residuals that signify anomalies and noise³⁸.

Noise removal

An approach referred to as the RSTL employs BF to eliminate noise. Smoothing techniques for the time series data $\{y_t\}_{t=1}^N$ BF achieves this through spatial and intensity-based weights, securing edge features while minimizing noise.

The following is the legalization of the concept Eq. (8)

$$y'_t = \sum_{j \in J} w_j^t y_j \quad (8)$$

where a window around ' t ' is defined by $J = \{t - H, \dots, t + H\}$ with width $2H + 1$. Two Gaussian functions are used to derive the weights w_j^t , Eq. (9).

$$w_j^t = \frac{1}{z} \exp \left(-\frac{(j-t)^2}{2\delta_j^2} \right) \exp \left(-\frac{|y_j - y_t|^2}{2\delta_i^2} \right) \quad (9)$$

Hence, the constants δ_d^2 and δ_i^2 are applied to standardize the spatial smoothing and intensity smoothing correspondingly. In addition, in order to verify that the aggregate of the weights = 1, the normalization factor $\frac{1}{z}$ is applied.

The time series is updated as the following Eq. (10) to Eq. (12) after using BF:

$$y'_t = \tau_t + s_t + r'_t \quad (10)$$

$$\text{where, } r'_t = a_t + (n_t - \hat{n}_t) \quad (11)$$

$$\text{and } \hat{n}_t = y_t - y'_t \quad (12)$$

is the representation of the filtered noise.

Trend extraction

Handling the complex interaction with the seasonality (s_t) embedded in the time series is required to extract the trend component (τ_t) in a SE prediction model. To attenuate seasonal impacts, the seasonal differencing is applied to the denoised data (y'_t) as follows, Eq. (13).

$$g_t = \nabla_T y'_t = y'_t - y'_{t-T} = \nabla_T \tau_t + \nabla_T s_t + \nabla_T r'_t \quad (13)$$

where the seasonal difference operation, $\nabla_T x_t = x_t - x_{t-T}$, captures the shift in data over a period T , while $\nabla x_t = x_t - x_{t-1}$ reflects the first-order difference.

The first-order differences of the trend, $\nabla \tau_t$ influenced the series g_t the seasonal and residual differences are typically less changeable than the trend. This work minimizes the following objective function to extract ' τ_t ' strongly, including first- and second-order differences, Eq. (14) and Eq. (15).

$$\sum_{t=T+1}^N \left| g_t - \sum_{i=0}^{T-1} \nabla \tau_{t-i} \right| + \lambda_1 \sum_{t=2}^N |\nabla \tau_t| + \lambda_2 \sum_{t=3}^N |\nabla^2 \tau_t| \quad (14)$$

$$\text{where } \nabla^2 \tau_t = \tau_t - 2\tau_{t-1} + \tau_{t-2} \quad (15)$$

It represents the second-order difference that captures rapid and slow changes in SE result data. The optimization is facilitated by formulating this objective function in a matrix form, Eq. (16)

$$\| g - M \nabla \tau \|_1 + \lambda_1 \| \nabla \tau \|_1 + \lambda_2 \| D \nabla \tau \|_1 \quad (16)$$

Here, \mathbf{g} and $\nabla \tau$ are vector representations of g_t and $\nabla \tau_t$. The Toeplitz matrices are \mathbf{M} and \mathbf{D} , which map the first and second differences across the series.

Seasonality extraction

The extraction of the seasonality component s_t following trend removal handles “*contaminated seasonality*” caused by residual data that includes shifted patterns and outliers³⁹. Numerous neighborhoods are considered by non-local seasonal filtering spanning multiple cycles, each positioned on data points $y_{(t-kT)}$, where the ‘ k ’ range is from 1 to K . There is an inclusion of $2H + 1$ data points surrounding each center, enabling a more complete assessment of seasonal patterns.

A weighted sum of the neighborhood values is the approximation of the seasonality, s_t , Eq. (17).

$$s_t'' = \sum_{(t',j) \in \Omega} w_{(t',j)}^t y_j'' \quad (17)$$

Weights $w_{(t',j)}^t$ are defined by Eq. (18).

$$w_{(t',j)}^t = \frac{1}{Z} \exp \left(-\frac{(t' - t)^2}{2\delta_d^2} - \frac{(y_{t''}'' - y_t'')^2}{2\delta_i^2} \right) \quad (18)$$

Higher weights, improving the strength of seasonality approximations against anomalies and seasonal changes, are ensured by this setup, where the points have the same seasonal features as y_t'' ,

Seagull optimization algorithm (SOA)

The seagulls attack the other birds by moving in a natural spiral form. Figure 2 illustrates a conceptual model of these features⁴⁰. The description of these behaviours can be done in such a way that links them to the objective function that requires improvement. This facilitates the birth of an improved SOA. This study mainly focuses on the behaviours of natural seagulls.

This algorithm stimulates the movement of a flock of seagulls from one place to another. During migration, seagulls should meet three requirements.

Avoiding collisions

In order to avoid collisions with other birds like seagulls, the position of a new Search Agent (SA) has been added with a variable \mathbf{A} (Fig. 3a), Eq. (19).

$$\vec{C}_s = \mathbf{A} \times \vec{P}_s(x) \quad (19)$$

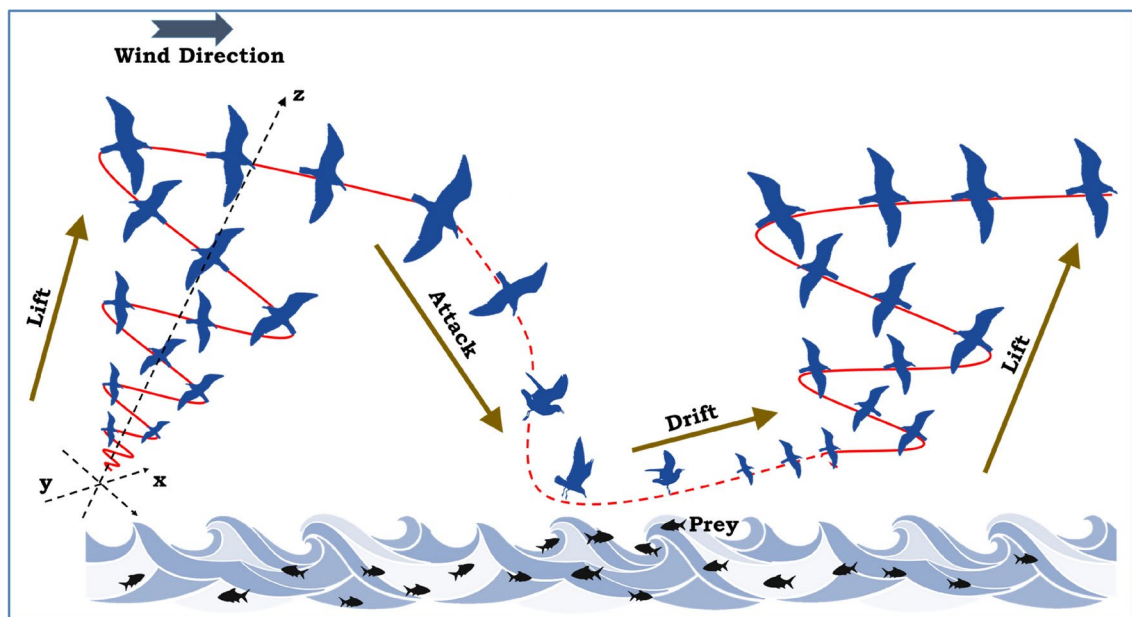


Fig. 2. The migration and spiral attack procedure of seagulls.

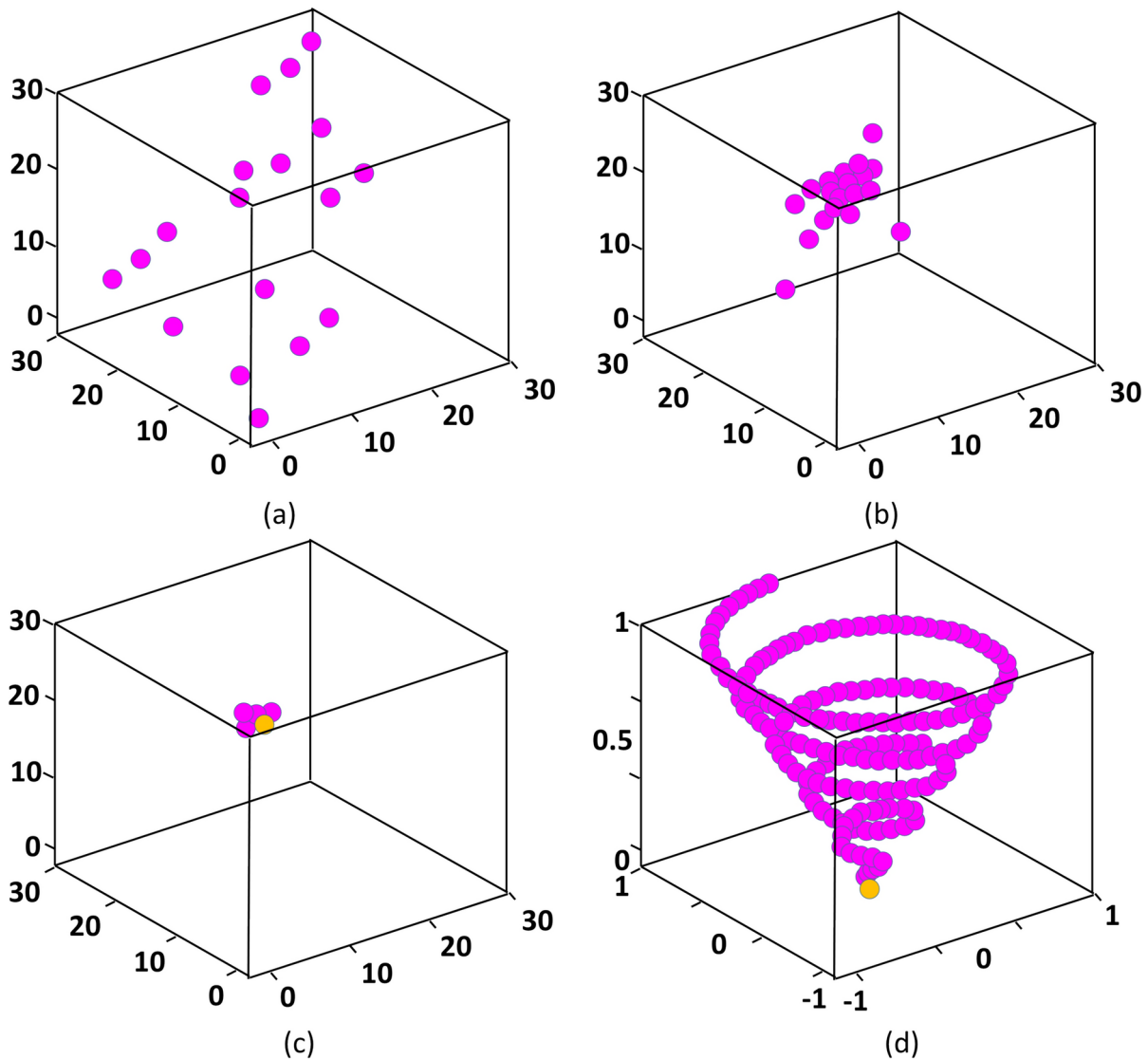


Fig. 3. (a) Collision avoidance between search agents; (b) Driving of search agents towards the best neighbor; (c) Convergence towards the search agent, and (d) Natural assaulting behavior of seagull.

where the current iteration is signified by ' x ', SA's movement behaviour in the specified search space is denoted by A , and the position of SA is denoted by \vec{C}_s , which prevents collision with other SAs. The current position of SA is denoted by \vec{P} , Eq. (20).

$$A = f_c - (x \times (f_c / \text{MaxIteration})) \quad (20)$$

where, $x = 0, 1, 2, \dots, \text{MaxIteration}$, When the frequency of utilization of variable ' f_c ' is introduced and linearly lowered from ' f_c ' to '0'. The value of ' f_c ' in this research work.

Movement towards best neighbor's direction

Once a collision with their neighbours is prevented, the SA move toward the best neighbour. (Fig. 3b), Eq. (21).

$$\vec{M}_s = B \times \left(\vec{P}_{bs}(x) - \vec{P}_s(x) \right) \quad (21)$$

where exploration and exploitation are balanced by the randomized behaviour of B , the positions of SA are represented by M_s , \vec{P}_{bs} , relative to the most appropriate SA, \vec{P}_{bs} (*i.e.*, fittest seagull). The following Eq. (22) determines B :

$$B = 2 \times A^2 \times rd \quad (22)$$

where in between [0, 1] lies the random number 'rd'. The position regarding the optimum SA can be modified by SA as depicted in Fig. 3c, Eq. (23).

$$\vec{D}_s = \left| \vec{C}_s + \vec{M}_s \right| \quad (23)$$

where the distance in SA is represented by \vec{D}_s , and it is appropriate for SA distances, that is the best seagull that has less FV.

Attacking (exploitation)

The exploitation intends to use the search's historical performance and experience. During migration, seagulls can alter their angle of attack and speed continuously. They use their wings and weight to maintain their height. Spiral movement occurs mainly in the wind as the predator attacks the prey (Fig. 3d).

The following describes this behaviour in the 'x', 'y', and 'z' planes, Eq. (24) and Eq. (27).

$$x' = r \times \cos(k) \quad (24)$$

$$y' = r \times \sin(k) \quad (25)$$

$$z' = r \times k \quad (26)$$

$$r = u \times e^{kv} \quad (27)$$

where the diameter of each spiral turn is 'r' and a random value between $[0 \leq k \leq 2\pi]$ is 'k'. Spiral shape variables are described by 'u' and 'v', while the base of the natural logarithm is represented by 'e'. The current position of SA is calculated using Eq. (28).

$$\vec{P}_s(x) = \left(\vec{D}_s \times x' \times y' \times z' \right) + \vec{P}_{bs}(x) \quad (28)$$

when SAs save the best result, $\vec{P}_s(x)$ modifies the rest of the places.

The generation of the proposed SOA's population is primarily done at random. Regarding the best SA, the SA's positions may change when the iteration is processed. The value of 'A' reduces linearly as from ' f_c ' to 0. Variable 'B' takes the responsibility for ensuring a smooth transition from exploration to exploitation.

Output: Optimal Search Agent \vec{P}_{bs}

- 1 Initialize the parameters A, B, and Max_Iteration
- 2 Set $f_c \leftarrow 2$
- 3 Set $u \leftarrow 1$
- 4 Set $v \leftarrow 1$
- 5 **While** $x < \text{Max_Iteration}$ **Do:**
 - $\vec{P}_{bs} \leftarrow \text{Compute_Fitness}(\vec{P}_{bs})$;
 - $rd \leftarrow \text{Rand}(0,1)$;
 - $k \leftarrow \text{Rand}(0,2\pi)$;
 - $r \leftarrow u \times e^{(k \times v)}$;
 - Calculate the distance \vec{D}_s ;
 - $\vec{P} \leftarrow x' \times y' \times z'$;
 - $\vec{P}_s(x) \leftarrow (\vec{D}_s \times \vec{P}) + \vec{P}_{bs}$
 - $x \leftarrow x + 1$;
- 6 **End While**
- 7 **Return** \vec{P}_{bs}
- 8 **End Procedure**

Algorithm 1: SOA Input: Population \vec{P}_s .

```

1 While true Do:
    •  $\text{FIT}_s[i] \leftarrow \text{Fitness\_Function}(\vec{P}_s(i,:));$ 
2 End Do
3 Return  $\text{FIT}_{s\_\text{best}}$ 
4 End Procedure

```

Algorithm 2: Compute_Fitness (\vec{P}_s).

```

1 Best  $\leftarrow \text{FIT}_s[0];$ 
2 While true Do:
    • If  $\text{FIT}_s[i] < \text{Best}$  Then
        • Best  $\leftarrow \text{FIT}_s[i];$ 
    • End If
3 End For
4 Return Best
5 End Procedure

```

Algorithm 3: BEST($\text{FIT}_s[]$).

Problem definition

Let D represent a dataset consisting of historical photovoltaic-Solar Energy (PV-SE) generation values and associated MF.

The dataset can be expressed as, Eq. (29)

$$D = \{(X_t, y_t) \mid t = 1, 2, \dots, T\} \quad (29)$$

where X_t is the feature vector at time t , including meteorological parameters such as solar irradiance (SI_t), temperature (Temp_t), and humidity (RH_t), and y_t is the observed PV-SE output at time t . The objective is to predict future PV-SE output y_{t+h} for a prediction horizon h , given past data. This prediction task is complicated by the inherent variability and noise in solar irradiance data, which is influenced by weather conditions, geographic location, and seasonal patterns.

Formally, the goal is to learn a predictive function f such that, Eq. (30)

$$\hat{y}_{t+h} = f(X_t, \theta) \quad (30)$$

where \hat{y}_{t+h} is the predicted PV-SE output and θ represents the parameters of the predictive model.

The challenge lies in handling the non-linear nature of y_t , managing noise and outliers, and ensuring the model generalizes well to unseen data. Additionally, the model must avoid issues like slow convergence and local minima, which are common in complex machine learning models.

Methodology

This section outlines the methodology for enhancing photovoltaic SE output prediction accuracy using advanced techniques. The ASOA is introduced as a dynamic optimization method to improve LSTM. ASOA modifies the traditional optimization algorithm by dynamically adjusting a modulation factor, allowing it to navigate the search space better and avoid premature convergence.

Additionally, RSTL divided time-series data into three distinct components: trend, seasonality, and residuals. Each component is then processed separately by ASOA-optimized LSTM, which ensures that each unique feature is captured effectively. The decomposition enhances the LSTM's ability to handle complex SE data, improving prediction accuracy.

Adaptive seagull optimization algorithm (ASOA)

The actual SOA formulation uses a linearly decreasing adaptation factor \mathbf{A} that may not be optimum for numerous problem landscapes. The primary problem is the chances of premature convergence or insufficient search space exploration, which may result in suboptimal solutions. To overcome the limitations, the ASOA is proposed; it is too firm when there is a linear decrease in \mathbf{A} , restricting the capacity of the algorithm to adjust to changes in the environment as the search advances.

Adaptive adjustment of ' \mathbf{A} '

Adapting \mathbf{A} in the context of ASOA entails inserting a modulation factor $M(x)$ that varies based on the algorithm's performance at each iteration. This change balances exploration and exploitation dynamically by responding to the algorithm's latest success in developing solutions.

The altered Eq. (31) for \mathbf{A} is:

$$\mathbf{A} = f_c - \left(x \times \frac{f_c}{\text{Max_iteration}} \times M(x) \right) \quad (31)$$

where:

- The primary value of \mathbf{A} is f_c , usually set to encourage broad exploration initially.
- The existing iteration number is denoted by $|x|$.
- Max_Iteration represents the sum of iterations scheduled for the algorithm.
- The modulation factor, which modifies the rate of decrease for \mathbf{A} , is $AM(x)$, ensuring the algorithm remains flexible.

Implementation of adaptive adjustment

The process commences with f_c , set to a value that initiates significant research. Simultaneously, $M(x)$ is initialized to 1. The progress in the algorithm's efficiency is monitored during each iteration. This requires monitoring the changes in the fitness of the algorithm's optimum solution. $M(x)$ is updated to reproduce the latest performance patterns. If no development is witnessed by the latest iterations in the best solution, $M(x)$ is reduced to slow down the decline of \mathbf{A} and promote the exploring skills for further research.

On the other hand, ' $M(x)$ ' is preserved or somewhat enhanced to expedite the exploitation of potential areas if there is improved and consistent performance. At each iteration, \mathbf{A} is recalculated with the freshly updated ' $M(x)$ ', enabling the algorithm to modify its search method dynamically. The adaptively adjusted \mathbf{A} is used in SOA's migration and exploration operations, increasing the algorithm's capability to successfully explore the search space and possibly find better global solutions.

ASOA optimized LSTM (ASOA + LSTM) model

The incorporation of ASOA for LSTM optimization comprises modifying several model parameters like the weights of the IG, FG, OG, and cell states. This method begins by stating the definition and starting of the LSTM parameters that will later be optimized. These contain the number of layers, units per layer, learning rate, and biases that can be set based on prior knowledge (or) heuristics. These parameters are optimized by applying ASOA, with the dynamically adjusted adaptation factor \mathbf{A} , as proved in Eq. 5.35.

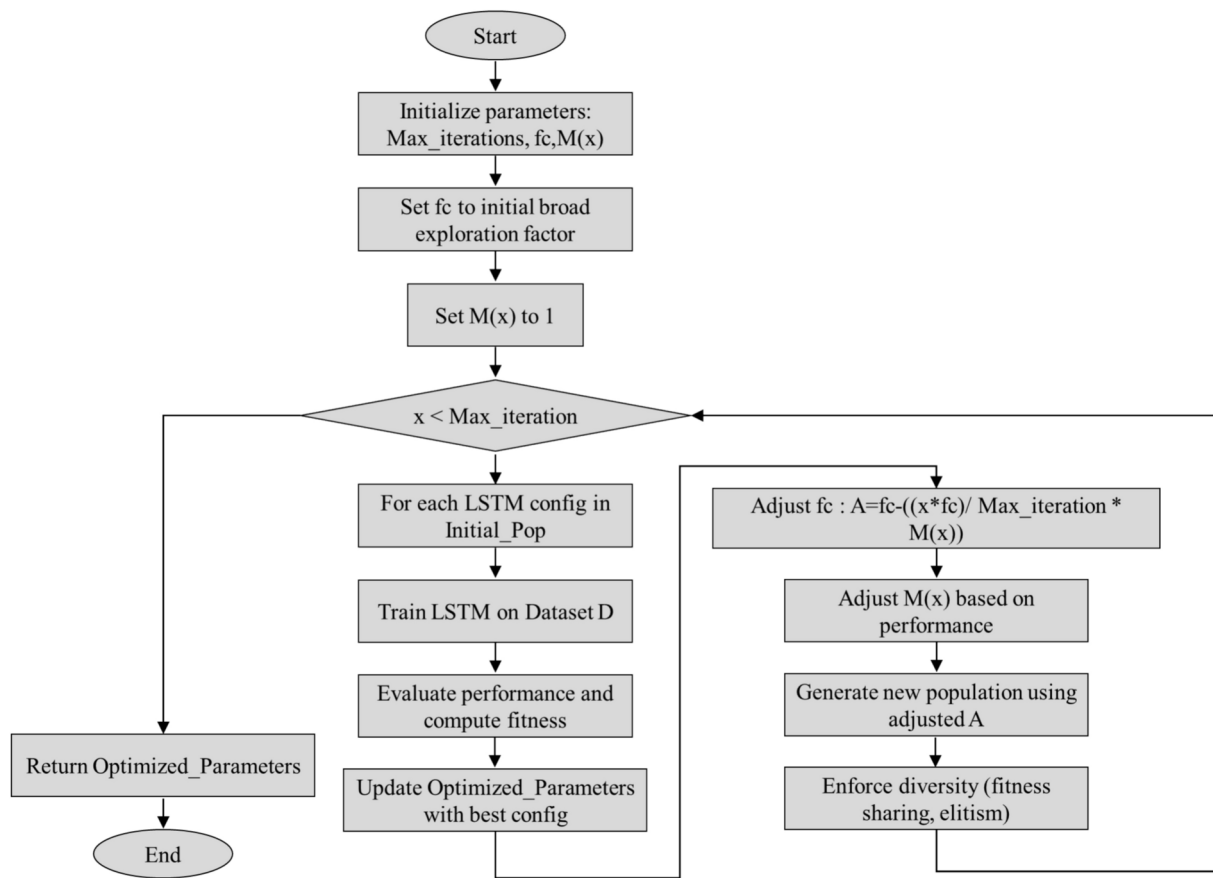
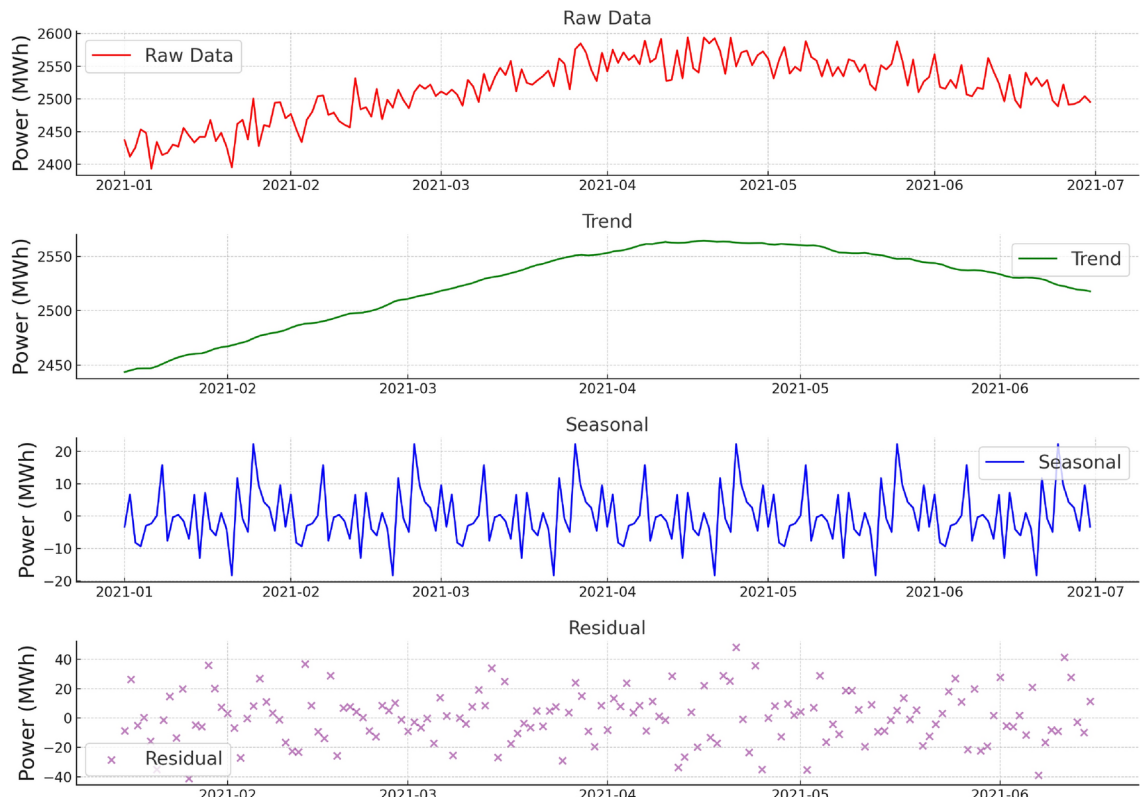
Following the latest progression of the algorithm, the modulation factor $M(x)$ adapts. If recent iterations have not improved, $M(x)$ is reduced to encourage exploration. Contrarily, inflating or maintaining $M(x)$ sheds light on exploitation when there is a consistent improvement in performance. This dynamic modification allows the algorithm to modify its search method efficiently. The fitness of each parameter set is decided by the performance of LSTM on a validation dataset that is usually predictable in terms of loss and accuracy. During this optimization phase, the exclusive update rules for the LSTM gates are used directly for the learning iterations of the model. Let the optimized parameters be denoted as $W_f^*, W_i^*, W_o^*, W_c^*, U_f^*, U_i^*, U_o^*, U_c^*, b_f^*, b_i^*, b_o^*, b_c^*$. In the LSTM Eq. (32) to Eq. (35)), the optimized parameters swap the real ones.

$$\text{FG : } f_t = \sigma (W_f^* x_t + U_f^* h_{t-1} + b_f^*) \quad (32)$$

$$\text{IG : } i_t = \sigma (W_i^* x_t + U_i^* h_{t-1} + b_i^*) \quad (33)$$

$$\text{OG : } o_t = \sigma (W_o^* x_t + U_o^* h_{t-1} + b_o^*) \quad (34)$$

$$\text{Cell Input Activation : } \tilde{C}_t = \tanh (W_c^* x_t + U_c^* h_{t-1} + b_c^*) \quad (35)$$

**Fig. 4.** Flowchart of the proposed ASOA + LSTM.**Fig. 5.** RSTL decomposition.

Input:

- **D:** Training dataset
- **Initial_Pop:** Initial population of LSTM configurations

Output: Optimized_Parameters: Optimized LSTM parameters**Procedure:****Step 1.** Initialize the parameters $Max_Iteration$, f_c (Initial broad exploration factor), and $M(x)$ **Step 2.** Set $f_c \leftarrow$ initial broad exploration factor**Step 3.** Set $M(x) \leftarrow 1$ (Initialize modulation factor)**Step 4. While** $x < Max_Iteration$ **Do:** **For Each** LSTM configuration in *Initial_Pop*: **Step 5.** Train LSTM with the current configuration on D **Step 6.** Evaluate performance to compute fitness **Step 7.** Update *Optimized_Parameters* with the best-performing LSTM configuration **Step 8.** Adjust f_c using: $A = f_c - \left(\frac{x \times f_c}{Max_Iteration} \times M(x) \right)$ **Step 9.** Adjust $M(x)$ based on performance feedback: *If there is no improvement in the last N iterations:*

- $M(x) \leftarrow 0.5$ (*Reduce the decrement rate of A to encourage exploration*)

Else

- $M(x) \leftarrow 1$ (*Maintain or increase exploitation focus*)

Step 10. Generate new population by applying migration and foraging behavior mimicked by SOA, using the adjusted A **Step 11.** Enforce diversity through mechanisms such as fitness sharing and elitism checks.**Step 12.** **End While****Step 13.** Return *Optimized_Parameters***Step 14.** **End Procedure**

Algorithm 4: ASOA + LSTM.

RSTL with ASOA optimized LSTM [RSTL + (ASOA + LSTM)] for PV ENERGY PREDICTION

The prediction process commences with data preprocessing, which includes cleaning, normalizing, and preparing raw data on PV-SE generation and other meteorological parameters for future study. Next to preprocessing, the ELNET-BDE approach proposed is used for FS. This method chooses the most appropriate features for the statistical significance and predictive capability-based prediction model. The FS, which contains observed and predicted data on SI, Atmospheric Temperature (AT), Relative Humidity (RH), and Cloud Cover (CC), is a necessary input that motivates prediction accuracy.

Once the essential FS is identified, the RSTL decomposes the data. RSTL classifies time series data into three different components (Fig. 5): seasonal component s_t that captures repeated cyclical patterns, trend component τ_t for longer-term development or modifications and residual r_t that contains irregular variations that are not compatible with seasonal or trend categories. Each of these components is considered a unique entity, demonstrating multiple parts of the underlying behaviours and features of data.

Individually, the decomposed components s_t , τ_t , and r_t are entered into their corresponding LSTM models, which the ASOA has optimized. The capability of LSTM is improved by this optimization approach for efficiently

managing the subtleties of each component. The ASOA utilizes the dynamic adjustment procedure to fine-tune the LSTM parameters, such as the IG, FG, and OG weights and biases. Using the Eq. (36), recalibrating the adaption factor \mathbf{A} is done in this process.

For their components \hat{s}_t , $\hat{\tau}_t$, and \hat{r}_t , LSTM models generate predictions. These predictions reveal the predictable seasonal patterns, trends, and residual predictions. There is a usage of these individual predictions in the final phase of the prediction process for generating the total PV-SE prediction \hat{y}_t . For each time point, ' t ' is expressed as Eq. (36).

$$\hat{y}_t = \hat{s}_t + \hat{\tau}_t + \hat{r}_t \quad (36)$$

The predictions from each component are integrated with this summation approach to give an inclusive and exact prediction of PV-SE output, leveraging the individual models' unique capabilities adapted to seasonal, trend, and residual patterns. Algorithm 5 presents the PV-SE prediction model using the RSTL with ASOA-LSTM.

Input: D: Dataset containing historical PV energy generation and MF.

Output: \hat{y}_t : Predicted PV energy result at each time t .

Procedure:

Step 1. Data Preprocessing

- Clean and normalize the dataset D .
- Standardize the features in D with a '0' mean and unit variance.

Step 2. FS using ELNET-BDE

- Apply ELNET-BDE to D to FS.
- Retain features with high Bayesian posterior density.

Step 3. Data Decomposition using RSTL: Decompose the FS into seasonal (s_t), trend (τ_t), and residual (r_t) components.

Step 4. Initialize LSTM: Set up separate LSTM for s_t , τ_t , and r_t .

Step 5. Optimize LSTM Models using ASOA

- **Define Initial Parameters:** f_c (Broad Exploration Factor), $M(x)$ (Modulation Factor), $Max_Iterations$
- **For Each Model** $\in \{\text{LSTM}_s, \text{LSTM}_\tau, \text{LSTM}_r\}$:
 - **For** $x = 1$ to $Max_Iterations$:
 - Train the model with the corresponding component.
 - Evaluate model performance using metrics such as RMSE or MAE.
 - Adjust the adaptation factor \mathbf{A} using: $A = f_c - \left(\frac{x \times f_c}{Max_iteration} \times M(x) \right)$
 - Update $M(x)$ based on performance feedback to enhance exploration or exploitation.
 - Update model parameters based on optimized values.

Step 6. Prediction Generation:

- **For Each** time point t :
 - \hat{s}_t = Prediction (LSTM_s, s_t)
 - $\hat{\tau}_t$ = Prediction (LSTM_τ, τ_t)
 - \hat{r}_t = Prediction (LSTM_r, r_t)
 - $\hat{y}_t = \hat{s}_t + \hat{\tau}_t + \hat{r}_t$

Step 15. Output: Return \hat{y}_t For all t .

Step 16. End

Algorithm 5: Forecast PV Power using RSTL with ASOA-Optimized LSTM.

The methodology presented integrates the ASOA + LSTM, optimized through RSTL, to tackle the challenges of PV-SE prediction. The dynamic adjustment of the ASOA ensures the adaptive balance between exploration and exploitation, which enhances the LSTM's capability to process the decomposed components—seasonal, trend, and residual. In the next section, the performance of the proposed model will be analyzed using the collected data, evaluating its effectiveness in addressing the complexities of solar energy forecasting.

Experimental analysis

Dataset

In this research work, two primary datasets were collected from a SE plant in Vishakhapatnam, India. The plant has generated electrical energy from 3.3 acres of agricultural land since 2017, employing polycrystalline panels. An installed capacity of 0.6 MW DC/0.5 MW AC contributes considerably to the city's energy mix, producing an estimated 0.892 million units of electricity per year and relocating around 607 tonnes of CO₂. The historical data collection spans three years, from 1st January 2020 to 31st December 2023, Figure 6 depicts the solar park's SE generation over the experimental study period.

To ensure the proposed model's generalization and avoid overfitting, the following strategies were implemented:

1. The dataset was divided into three subsets:
 - *Training Set* (85%) Used for model learning.
 - *Validation Set* (10%) Used for hyperparameter tuning and early stopping.
 - *Testing Set* (5%) Used for final evaluation on unseen data.
2. Each experiment was repeated three times to verify the consistency and reliability of the results. The mean and standard deviation of performance metrics (RMSE, MAE, and R₂) were reported to reflect the variability in performance.
3. The dataset spans three years (2020–2023), covering various meteorological conditions, seasonal patterns, and diverse weather scenarios. This ensures the model encounters a wide range of real-world conditions, enhancing its ability to generalize effectively.

In addition, this work used both experimental and predicted meteorological data in our research. The observed data are attained via a dedicated meteorological tower equipped with strategically installed sensors that measure: Solar Irradiance (SI), Temperature (Temp) and Dew Point (DP), Relative Humidity (RH), Wind Speed (WS) and Wind Direction (WD), Atmospheric Pressure (AP), Precipitation (Precip), Cloud Cover (CC), Global Horizontal Irradiance (GHI), Direct Normal Irradiance (DNI), and Diffuse Horizontal Irradiance (DHI). The Indian Meteorological Department (IMD) provides predicted meteorological data. This prediction data covers the same period as the experimental data and contains predictions of significant meteorological variables like (i) Atmospheric Temperature, (ii) Precipitation, (iii) Relative Humidity, (iv) Wind Speed and Direction, (v) Cloud Cover, (vi) Solar Irradiance, (vii) Atmospheric Pressure, (viii) Visibility, (ix) Dew Point and (x) UV Index.

Most significantly, the actual and projected datasets include a daily time ranging from 00:00 to 23:59 IST. The experimental meteorological parameters used in SE prediction research are shown in Table 1, including their abbreviations and units. Table 2 shows the predicted variables attained from IMD.

Data preprocessing

In identifying missing data from SE output and MF monitoring between January 2020 and December 2023, a detailed analysis using Python's Panda library revealed approximately 4% missing AT and 2% missing SE values, likely due to technical or systematic errors during specific weather conditions. Various imputation methods were applied to address this: The predictive Imputation Method (PIM) used linear regression models based on related variables, the Time Series Imputation Method (TSIM) utilized linear interpolation and seasonal decomposition, and the Mean Imputation Method (MIM) applied the mean of existing values for minor gaps. Each method was verified post-implementation to ensure the integrity of the dataset. Outlier detection was conducted using Box Plots and Z-scores to identify and statistically confirm data points outside normal ranges visually. Outliers were corrected using adjacent data or removed entirely if they represented true anomalies.

Additionally, error identification combined automated checks for extreme values with manual reviews of suspicious data against system logs and environmental records, applying corrections or flagging data as needed. To ensure data consistency, timestamps were standardized to Coordinated Universal Time (UTC), measurements were uniformly resampled, and units of measurement were standardized across the dataset. Cross-variable validations were performed to confirm the logical consistency of data correlations, ensuring that higher solar irradiance values corresponded to expected SE outputs and temperature ranges. Table 3 presents the dataset description.

Experimental setup

The experiments were conducted on a high-performance computing system equipped with an Intel Core i7 processor (10th Generation) running at 3.8 GHz, 64 GB of DDR4 RAM, and an NVIDIA GeForce GTX 1080 Ti GPU with 11 GB of GDDR5X memory. The software environment was based on Python 3.8, utilizing key libraries such as TensorFlow for training and optimizing the LSTM-NN, Pandas for data manipulation, and Matplotlib for visualization. All experiments were executed on a 64-bit Windows 10 operating system. The experimental model in this research work aims to assess the ASOA's efficiency in optimizing LSTM for SE prediction. The dataset, which includes historical SE data and critical MF collected over three years from an SE

facility, is pre-processed to remove anomalies and standardize the data. Since the Huber loss function is robust against data outliers, it is used in the LSTM. By dynamically modifying modulation factor $M(x)$ based adaption factor A, ASOA improves optimization. Based on the model's performance, the factor is recalibrated at each iteration, starting with an initial learning rate of 5×10^{-5} and an initial broad exploration factor f_c for enabling a wide range of parameter exploration.

For balancing computational efficiency and dynamic response, a batch size of 48 is trained with an initial stopping mechanism, which halts training in case there is no improvement in the validation loss for 10 consecutive epochs, thus avoiding overfitting. To ensure a large dataset for training, simultaneously providing relevant data for validation and unbiased testing, the data are intentionally separated into training, validation, and testing segments with ratios of 85%, 10%, and 5%, respectively.

Computationally intense LSTM training and evaluation are evaluated by High-performance NVIDIA A100 GPUs. Each training session is repeated three times to validate the results' reliability and consistency. Performance metrics such as RMSE, MAE, and MAPE are used to evaluate the models. This inclusive configuration exploits ASOA's strong point in optimizing LSTM parameters, improving prediction accuracy, and creating a strong setup for advanced RE prediction applications. Table 4 contains the parameters along with their values.

Performance metrics

Three essential criteria evaluate RSTL's accuracy and predictive quality with the ASOA-optimized LSTM in predicting SE generation:

- (A) *RMSE* It is the square root of the average squared difference between predicted and actual values. Primarily, it is susceptible to massive errors, showing substantial differences in the model's predictions.

$$\text{RMSE} = \sqrt{\frac{1}{n} \sum_{i=1}^n (y_i - \hat{y}_i)^2} \quad (37)$$

- (B) *MAE* The average magnitude of prediction errors is computed by MAE without considering their direction. Since it maintains the same units as the data and is less sensitive to outliers than RMSE, it is easier to interpret

$$\text{MAE} = \frac{1}{n} \sum_{i=1}^n |y_i - \hat{y}_i| \quad (38)$$

- (C) *R*² The capability of independent variables to predict the dependent variable's variance is shown by R^2 , a statistical measure. The possibility of the model to predict unknown samples is indicated by R^2 with 1 signifying perfect prediction

$$R^2 = 1 - \frac{\sum_{i=1}^n (y_i - \hat{y}_i)^2}{\sum_{i=1}^n (y_i - \bar{y})^2} \quad (39)$$

In the comparative analysis, the proposed model incorporating the (RSTL + (ASOA + LSTM)), was compared with other model configurations to assess its performance in PV-SE prediction. Here's a precise overview of each model configuration utilized in the comparison:

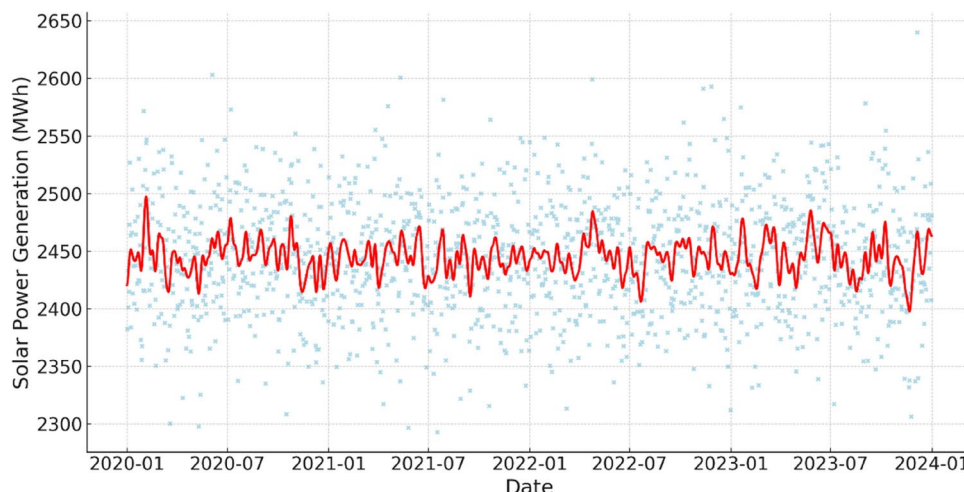


Fig. 6. Energy generation during the study period.

Parameter name	Abbreviation	Unit	Measurement Device
SI	SI	W/m ²	Pyranometers
Temperature	Temp	°C	Thermometers
Dew point	DP	°C	Hygrometers
Humidity	RH	%	Hygrometers
Wind speed	WS	m/s	Anemometers
Wind direction	WD	Degrees (°)	Wind vanes
Atmospheric pressure	AP	Hectopascals (hPa)	Barometers
Precipitation	Precip	Millimeters (mm)	Rain gauges
Cloud cover	CC	Okta (0–8 scale)	Ceilometers
Global horizontal irradiance	GHI	W/m ²	Solar radiometers
Direct normal irradiance	DNI	W/m ²	Solar radiometers
Diffuse horizontal irradiance	DHI	W/m ²	Solar radiometers

Table 1. Experimental MF.

Parameter name	Abbreviation	Unit
Temperature	Temp	°C
Precipitation	Precip	mm
Humidity	RH	%
Wind speed	WS	km/h
Wind direction	WD	Degrees (°)
Cloud cover	CC	Okta
SI	SI	W/m ²
Atmospheric pressure	AP	hPa
Visibility	Vis	km
Dew point	DP	°C
UV Index	UV	Index (1–11 +)

Table 2. Predicted MF.

- i. *STL + LSTM* This model decomposes the time series data using STL, which is later predicted with the help of a standardized LSTM. Compared to RSTL, STL is not very strong against outliers and unexpected changes.
- ii. *RSTL + LSTM* Same as the first; however, it employs RSTL that integrates methods for effectively managing outliers and unexpected changes and uses conventional LSTM to predict the decomposed components.
- iii. *STL + (SOA + LSTM)* By optimizing the LSTM parameters, this configuration refines the STL + LSTM using the standard SOA, targeting to enhance the performance of LSTM while processing decomposed data.
- iv. *STL + (ASOA + LSTM)* This model, an extension of the STL + LSTM, uses the ASOA to optimize LSTM parameters, giving dynamic adaption capacity, which may result in optimum optimization outcomes than the regular SOA.
- v. *RSTL + (SOA + LSTM)* This integrates the strength of RSTL decomposition with the optimization capabilities of SOA applied to the LSTM, intending to balance the advantages of robust data decomposition with effective parameter optimization.
- vi. *RSTL + (ASOA + LSTM) (Proposed)* Using RSTL for data decomposition and ASOA for optimizing the LSTM parameters is a highly advanced configuration. Using robustly deconstructed data components, the adaptive feature of ASOA is anticipated to improve the ability of LSTM to predict correctly.

Result analysis: actual vs prediction

Figure 7 compares actual and predicted SE output from multiple model configurations employed for PV-SE prediction, demonstrating their training in capturing the complexities of SE data. The STL + LSTM exhibits significant disparities between actual and anticipated outputs, showing that the model struggles to capture the peaks and channels of SE data. This highlights that the STL + LSTM challenges successfully identifying the highs and lows of SE data, as demonstrated by a finding that there are significant variances in the accurate and predicted results when applying the framework. This shows how conventional LSTM may have difficulty addressing the number of variables and complexity in SE results when STL decomposition is implemented for dividing the data, resulting in significant prediction errors.

The RSTL + LSTM, on the alternative tandem, displays greater coherence between the actual data and the predicted data than the STL + LSTM setup provides. The boost is probably owed to the adaptability of the RSTL, which is higher when dealing with significant outliers and unexpected changes. Considering specific abnormalities at the peak periods, this robust decomposition presents the LSTM with a more accurate and stable

	Variable name	Abbreviation	Unit
1.	Date	N/A	N/A
2.	SI (experimental)	SI _o	W/m ²
3.	SI (prediction)	SI _f	W/m ²
4.	Temperature (experimental)	T _o	°C
5.	Temperature (prediction)	T _f	°C
6.	Humidity (experimental)	RH _o	%
7.	Humidity (prediction)	RH _f	%
8.	WS (experimental)	WS _o	m/s
9.	WS (prediction)	WS _f	m/s
10.	Wind direction (experimental)	WD _o	Degrees (°)
11.	Wind direction (prediction)	WD _f	Degrees (°)
12.	Precipitation (experimental)	Precip _o	mm
13.	Precipitation (prediction)	Precip _f	mm
14.	Cloud cover (experimental)	CC _o	Okta (0–8 scale)
15.	Cloud cover (prediction)	CC _f	Okta (0–8 scale)
16.	Atmospheric pressure (experimental)	AP _o	Hectopascals (hPa)
17.	Atmospheric pressure (prediction)	AP _f	Hectopascals (hPa)
18.	Energy output	P _o	MWh

Table 3. Dataset description.

Hyperparameter	Value
Learning rate	5×10^{-5}
Adaptation factor (fc)	2
Modulation factor ($M(x)$)	Initially set to 1
Batch size	64
Early stopping	After 10 epochs without improvement
Epochs	100
Optimizer	RMSprop
Loss function	Huber loss
Data split	85%/10%/5%
Number of LSTM layers	3
Units per layer	150 per layer
Activation function	Sigmoid for gates, tanh for cell activations
Sequence length	24 (hours for daily cycle)
Dropout rate	0.3
Recurrent dropout rate	0.3

Table 4. Hyperparameter values.

database, allowing it to develop more accurate predictions. STL+(SOA + LSTM) and STL+(ASOA + LSTM) are both instances of models that employ optimization algorithms, and both of these models exhibit distinct degrees of enhanced performance at numerous phases. The ASOA-enhanced simulations, in particular, provide an improved visualization of the actual data patterns and changes. The evidence provided here indicates that the adaptive features of ASOA, which proactively fine-tune the variables of the LSTM, perform an integral part in improving the accuracy of the simulation model by proactively optimizing the exploration and exploitation balance during the learning phase. Considering all possible setups, the RSTL+(ASOA + LSTM) paradigm that has been developed will probably perform better than the model it replaced. In order to attain high prediction accuracy, reliable data processing is integrated with the dynamic optimization of variables. The visualization indicates that this model is more significant in its capacity to modify and predict in a highly unpredictable atmosphere. The prediction is achieved by accurately depicting the general trend and variations in the seasons, and its performance closely corresponds to the actual data values.

Result analysis: RMSE

The main objective of this statistical analysis is to assess the proposed RSTL+(ASOA + LSTM) in the context of several prediction models to predict the results of PV-SE. RMSE results from the training, validation, and test datasets, as shown in Figs. 8, 9, and 10, are employed to assess and contrast the models' performance. The

primary emphasis focuses on the proportion of increases achieved compared to the models used as the baseline. The RSTL + (ASOA + LSTM) that was recommended achieves the highest possible performance, as demonstrated by the following median RMSE values: training 7.941 with an STD of 1.615, validation 7.768 with an STD of 1.616, and testing 8.734 with an STD of 1.718. These findings reveal a considerable decrease in prediction error, demonstrating the efficacy of robust decomposition and AO (Table 5).

The proposed model demonstrates a significant increase over the STL with a training mean RMSE, validation mean RMSE, and testing mean RMSE of 9.451, 9.713, and 9.813, respectively. The proposed model particularly curbs the training RMSE, validation RMSE, and testing RMSE by 15.97%, 20.03%, and approximately 11.00%. When comparing the proposed model to the standalone LSTM, which has mean RMSE of training, validation, and testing of 8.761, 9.195, and 9.254, respectively, the improvements are similarly noticeable. The proposed model RMSE reduces the training, validation, and testing by an approximation of 9.34%, 15.53%, and 5.62%. For the STL + LSTM, the mean RMSE which has a training, validation, and testing of 8.756, 9.061, and 9.236, respectively, the proposed model improves RMSE by approximately 9.29%, 14.28%, and 14.28% in the training, validation, and testing.

The RSTL + LSTM model, which had RMSE as a training, validation, and testing mean of 8.603, 8.993, and 9.233, respectively, outperformed the proposed model. The improvements of RMSE are around 7.68%, 13.61%, and 5.40% for the training, validation, and testing. Compared to the STL + (SOA + LSTM), which achieves RMSE mean of training, validation, and testing of 8.618, 8.425, and 9.119, the proposed model enhances RMSE roughly by 7.85%, 7.80%, and 4.23% in the training, validation, and testing. The proposed model also outperforms the STL + (ASOA + LSTM) mean RMSE, which has a training, validation, and testing of 8.503, 8.682, and 9.098, respectively. The RMSE of training, validation, and testing have improved by approximately 6.63%, 10.53%, and 4.00%. Eventually, when compared to the RSTL + (SOA + LSTM), the RMSE mean, which has a training, validation, and testing of 8.184, 8.121, and 9.101, respectively, the proposed model improves by roughly 2.97% in training, 4.34% in validation, and 4.03% in the test.

Result analysis: MAE

In the following section of the work, the developers analyze the accuracy of the RSTL + (ASOA + LSTM) that has been proposed by considering various MAE values, as shown in Figs. 11, 12, and 13. In the assessment, the results of the training, validation, and test datasets are all considered for attention. Furthermore, the proposed approach is compared to different models, and percentage boosts in prediction accuracy are notably emphasized. With mean MAE training, validation, and testing ranging from 0.898 (STD:0.414), 0.868 (STD:0.409), and 0.868 (STD:0.437, respectively, the RSTL + (ASOA + LSTM) framework that has been proposed performs very effectively (Table 6). This research proves that the algorithm performs well in reducing the number of errors that result in predictions by employing reliable decomposition and AO methodologies.

When compared to the STL, which has mean values of MAE of 1.198, 1.312, and 1.437 training, validation, and testing, the proposed model enhanced considerably. There is a decrease of MAE of 25.04%, 33.84%, and 39.58% in training, validation, and testing. The standalone LSTM model that contains mean MAE is a training, validation, and testing of 0.954, 1.024, and 1.123, respectively, which falls short of the proposed model. The experimental improvements in MAE are 5.87%, 15.24%, and 22.64% in training, validation, and testing, demonstrating the increased value of AO.

During training, validation, and testing, the mean MAE for the STL + LSTM is 0.932, 1.002, and 1.101. The proposed model performs better MAE, with 3.65%, 13.36%, and 21.15% lower training, validation, and testing, showing the benefits of RSTL and ASOA. The proposed model also outperforms the RSTL + LSTM configuration with a mean MAE of 0.919, 0.989, and 1.099 for training, validation, and testing. The MAE reductions are 2.29%, 12.23%, and 20.92% for training, validation, and testing, highlighting the uses of adaptive models.

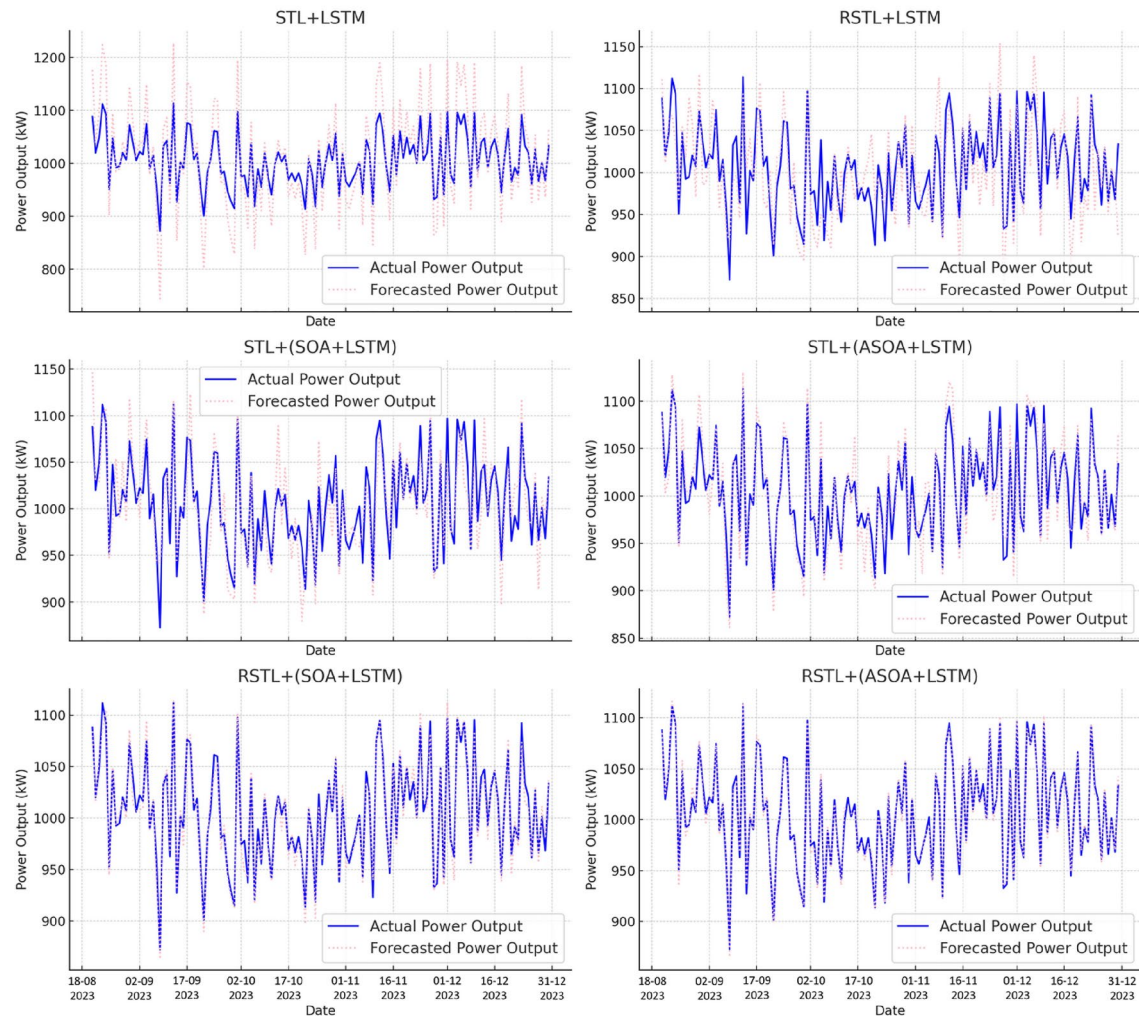
When compared to the STL + (SOA + LSTM) that improves the MAE mean value of training, validation, and test of 0.927, 0.997, and 1.096, respectively, the proposed model outperforms, showing increased performance of MAE is 3.13%, 12.97% and 20.73% in training, validation, and test, indicating ASOA's superior performance over SOA. The STL + (ASOA + LSTM) model mean MAE has 0.914, 0.936, and 1.033 for training, validation, and testing, and it is also less successful than the proposed model. The proposed model has MAE values that are 1.75%, 7.73%, and 19.02% lower in training, validation, and test datasets. Eventually, the RSTL + (SOA + LSTM) has a mean MAE of 0.907 during training, 0.903 during validation, and 1.022 during testing. The proposed model improves MAE results, reducing training by 1.00%, validation by 3.88%, and testing by 18.63%.

Result analysis: R^2

This section of the research work assesses the proposed RSTL + (ASOA + LSTM) performance by applying the R^2 metric that approximations measure how well regression predictions are apt for fundamental data points. Higher R^2 values propose improved prediction accuracy. The proposed model's R^2 values across training, validation, and test datasets, as shown in Figs. 14, 15, and 16, are compared to distinct baseline models, signifying percentage improvements as needed. Among all models, the most significant R^2 values are achieved by the proposed RSTL + (ASOA + LSTM), illustrating superior capacity for capturing variability in data. 0.808 is the training mean R^2 with an STD of 0.017, whereas 0.801 is the validation mean R^2 with an STD of 0.016. 0.804 is the test mean R^2 with an STD of 0.018. It should be noted that such large numbers can accurately predict PV-SE generation and provide proof of the model's accuracy and lifetime (Table 7).

A substantial rise in accuracy can be experimental with the model being considered compared to the STL, which has an R^2 mean value of training of 0.720, validation of 0.702, and test of 0.683. In the training, validation, and test datasets, the coefficients for R^2 of the model proposed to demonstrate a boost of 12.22%, 14.12%, and 17.71%, respectively. The successful implementation of the reliable seasonal-trend decomposition and adaptive optimizing methods recommended in the predictive model is an obvious instance of all these improvements.

Comparison of Actual vs. Forecasted Power Output by Model

**Fig. 7.** The actual vs prediction comparison for the compared models.

The LSTM, which achieved mean coefficients for R^2 of 0.771, 0.763, and 0.756 for training, validation, and testing, has been contrasted to the hypothesized model, which displays significant improvements above the present model. The increases in R^2 coefficients for the training, validation, and testing comprise primarily 6.35%, 4.80%, and 4.98%, respectively. The comparison above demonstrates how the introduction of RSTL + ASOA into the LSTM model contributes to a boost in the predictive accuracy of the overall model.

Mean R^2 coefficients for the STL + LSTM are 0.783, 0.767, and 0.761, correspondingly throughout the method's training, validation, and testing phases. When compared to this combination of factors, the proposed model is more effective, considering that it increases training R^2 coefficient by 3.19%, validation R^2 by 4.43%, and testing R^2 by 5.65%. The findings highlight the numerous advantages that can be attained from employing AO and reliable decomposition. Considering that the model's mean R^2 value presents a training of 0.791, a validation of 0.791, and a testing of 0.76, the issue endures performing exceptionally well. The training, validation, and testing R^2 increased by 2.15%, 1.26%, and 5.10%. This shows that, even with more robust seasonal-trend decomposition, the addition of ASOA enhances model performance considerably.

When the proposed and STL + (SOA + LSTM) were compared, the latter achieved R^2 mean training of 0.789, validation of 0.789, and testing of 0.763; the proposed model showed significant improvements. There has been an increase R^2 of up to 2.41% in training, 1.52% in validation, and 5.37% in testing. ASOA's superiority over SOA was demonstrated in this comparison when optimizing LSTM parameters. The STL + (ASOA + LSTM) contains 0.790 mean R^2 values for training, 0.793 for validation, and 0.787 for testing. 2.28%, 1.01%, and 2.16% are the improvement score of training, validation, and test R^2 , respectively. This shows the extra benefits achieved by combining RSTL and ASOA. The proposed model outdoes the RSTL + (SOA + LSTM) that contains mean values of 0.798, 0.797, and 0.790 for training, validation, and test R^2 , respectively. R^2 values increase by 1.25%, 0.50%, and 1.77% for training, validation, and testing, respectively. These improvements demonstrate using ASOA over SOA when combined with robust seasonal-trend decomposition.

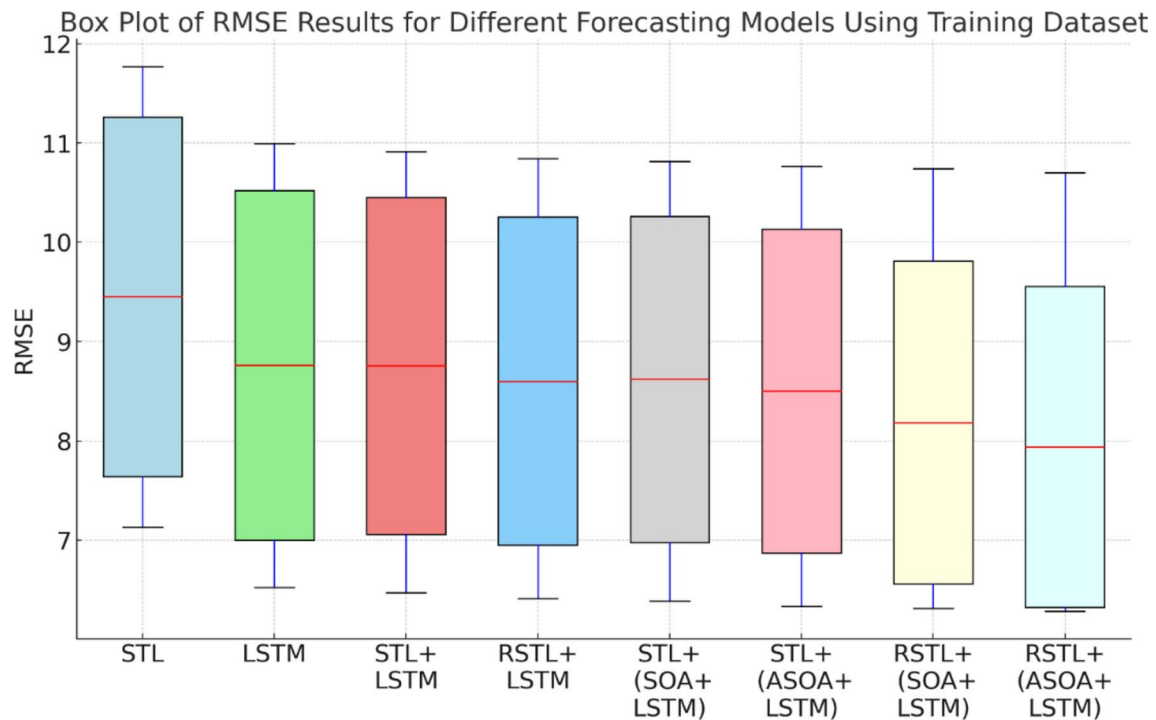


Fig. 8. RMSE for the training dataset.

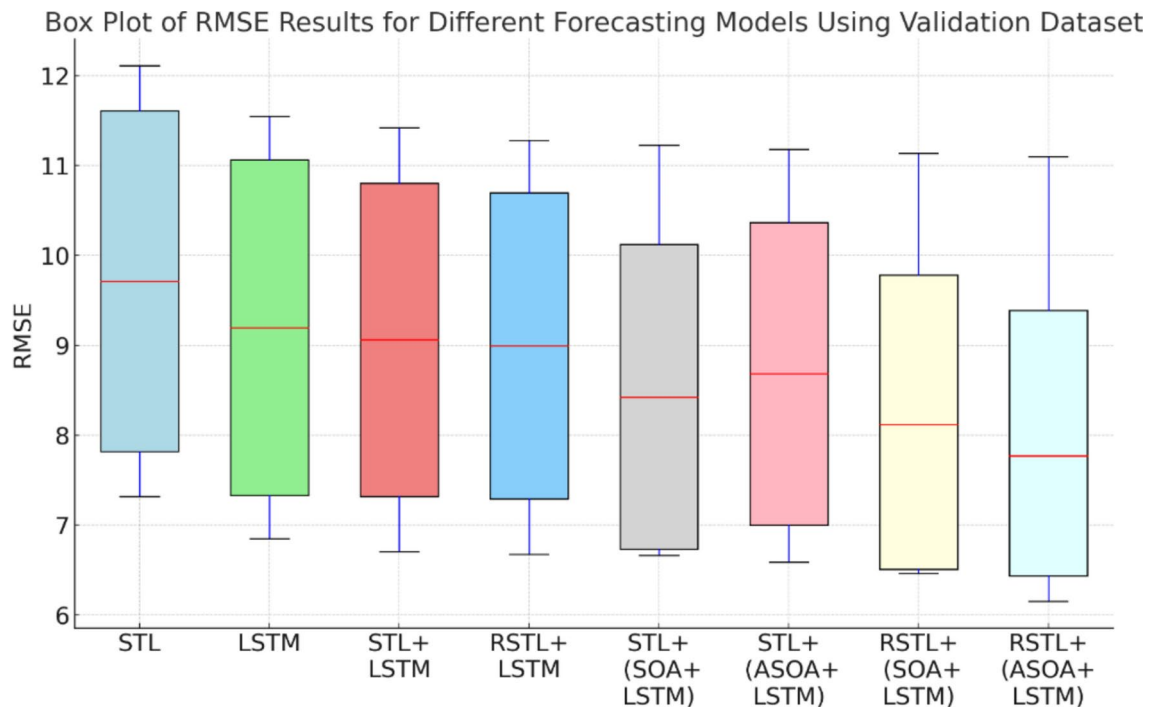


Fig. 9. RMSE for validation dataset.

Residual component autoregressive property analysis

An analysis was conducted to determine whether the residual component, following STL decomposition, exhibits autoregressive properties. The Ljung-Box test yielded a p-value of 0.015, which is below the 0.05 significance level, indicating statistically significant autocorrelation within the residuals. This result suggests that the residual component retains inherent patterns that may benefit from an autoregressive model. Additionally, Partial Auto-

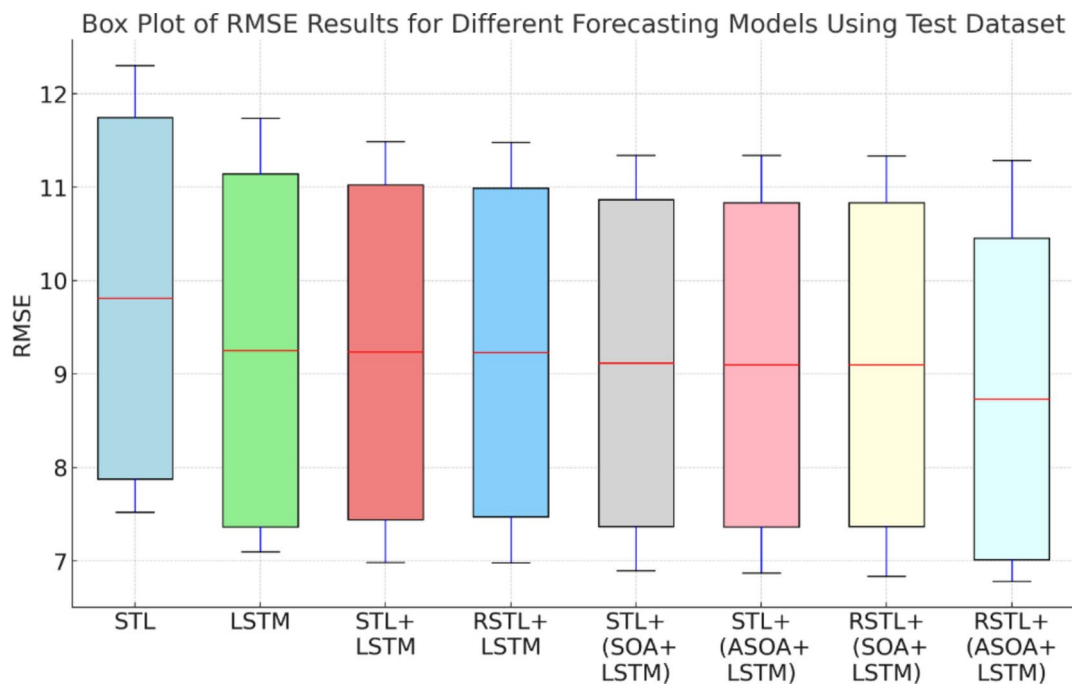


Fig. 10. RMSE for testing dataset.

Predictor	Train Min	Train Max	Train Mean	Train STD	Val Min	Val Max	Val Mean	Val STD	Test Min	Test Max	Test Mean	Test STD
STL	7.133	11.769	9.451	1.809	7.318	12.109	9.713	1.897	7.524	12.301	9.813	1.934
LSTM	6.523	10.998	8.761	1.761	6.847	11.543	9.195	1.865	7.098	11.739	9.254	1.891
STL + LSTM	6.472	10.912	8.756	1.698	6.706	11.417	9.061	1.742	6.983	11.489	9.236	1.791
RSTL + LSTM	6.413	10.843	8.603	1.652	6.672	11.281	8.993	1.702	6.98	11.478	9.233	1.758
STL + (SOA + LSTM)	6.385	10.812	8.618	1.643	6.661	11.224	8.425	1.695	6.899	11.339	9.119	1.749
STL + (ASOA + LSTM)	6.332	10.765	8.503	1.631	6.588	11.176	8.682	1.683	6.871	11.341	9.098	1.735
RSTL + (SOA + LSTM)	6.315	10.742	8.184	1.627	6.508	11.134	8.121	1.658	6.838	11.338	9.101	1.73
RSTL + (ASOA + LSTM)	6.284	10.701	7.941	1.615	6.435	11.101	7.768	1.616	6.783	11.285	8.734	1.718

Table 5. RMSE results for different prediction models.

Correlation Function (PACF) values at lags 1, 2, and 3 were observed to be 0.58, 0.45, and 0.31, respectively, reflecting moderate to weak autocorrelation across these lags (Table 8).

These findings support using an LSTM model for the residual component, as the moderate level of autocorrelation aligns with LSTM's capacity to capture temporal dependencies. However, if future analyses reveal purely stochastic characteristics in the residuals, a model such as GARCH may offer improved accuracy. This approach justifies a consistent LSTM model across trend, seasonal, and residual components, ensuring a straightforward structure without compromising predictive performance.

Discussion

This study presents an innovative integration of RSTL and ASOA to optimize LSTM and improve SE prediction accuracy. This approach's novelty lies in its unique design features and demonstrated performance improvement over traditional and hybrid models.

Design innovation

1. RSTL for improved data decomposition.

- Traditional decomposition techniques like STL struggle to handle high variability and noise in SE data, which can lead to substantial prediction errors. The RSTL technique enhances decomposition by accurately handling outliers, noise, and seasonal shifts, ensuring that the LSTM model is fed with cleaner, more structured data.

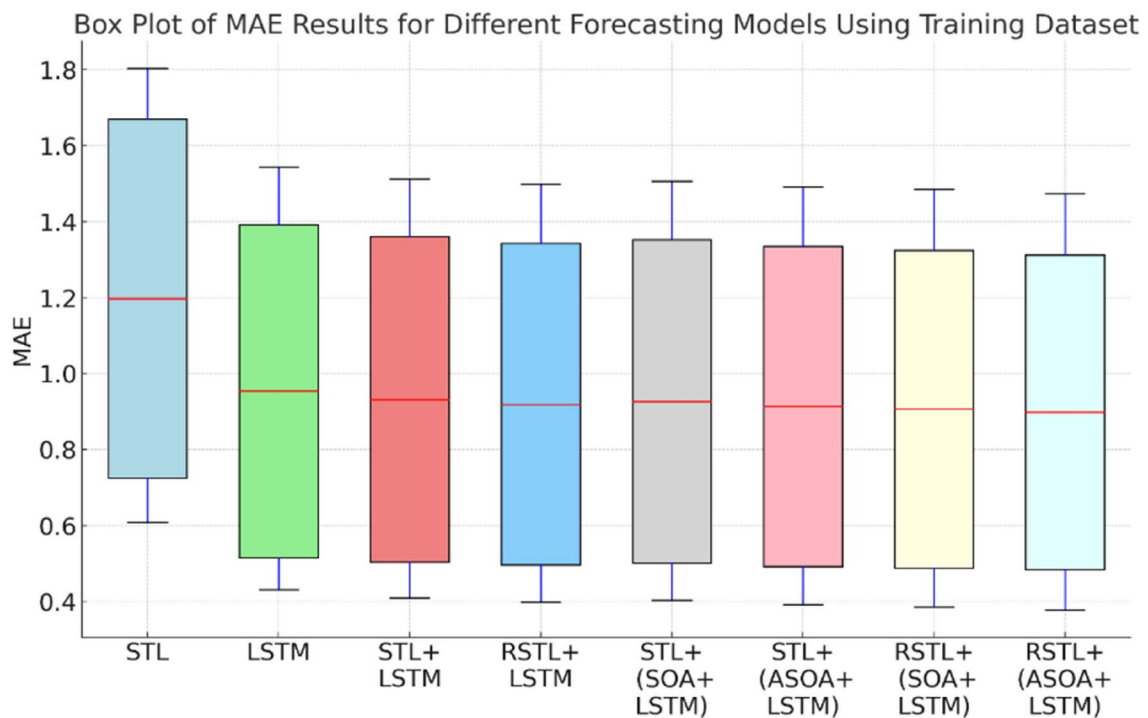


Fig. 11. MAE for training dataset.

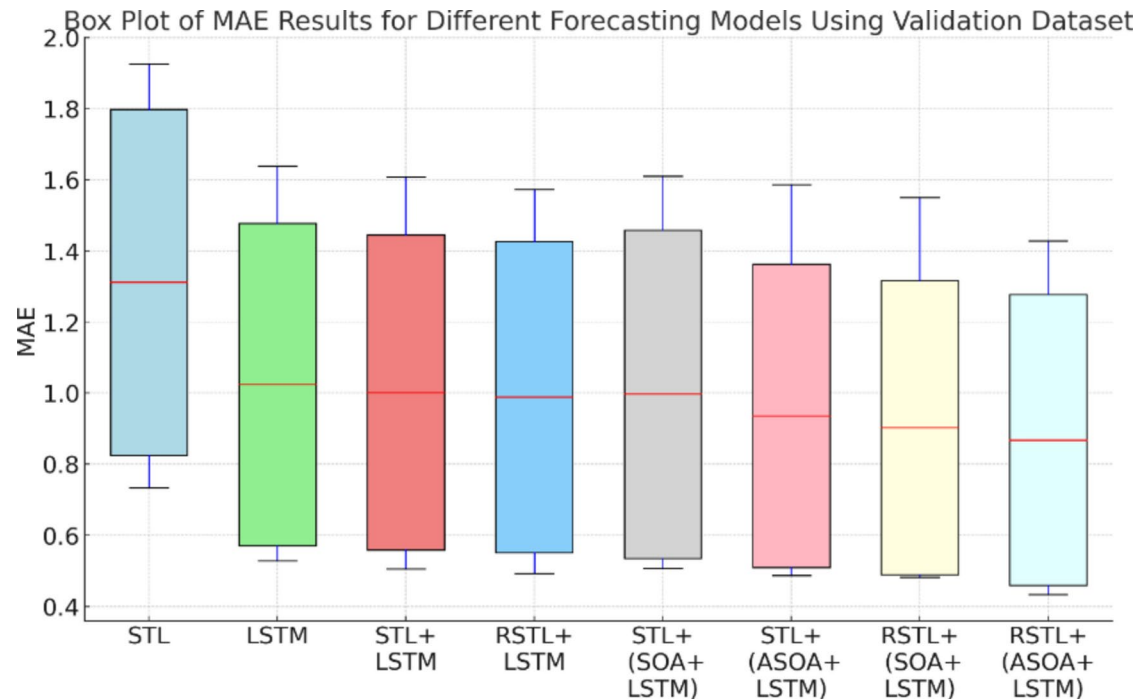


Fig. 12. MAE for validation dataset.

- This method improves the LSTM's ability to focus on distinct components—seasonal patterns, long-term trends, and irregular residuals—allowing for more targeted predictions for each aspect of solar energy fluctuations.

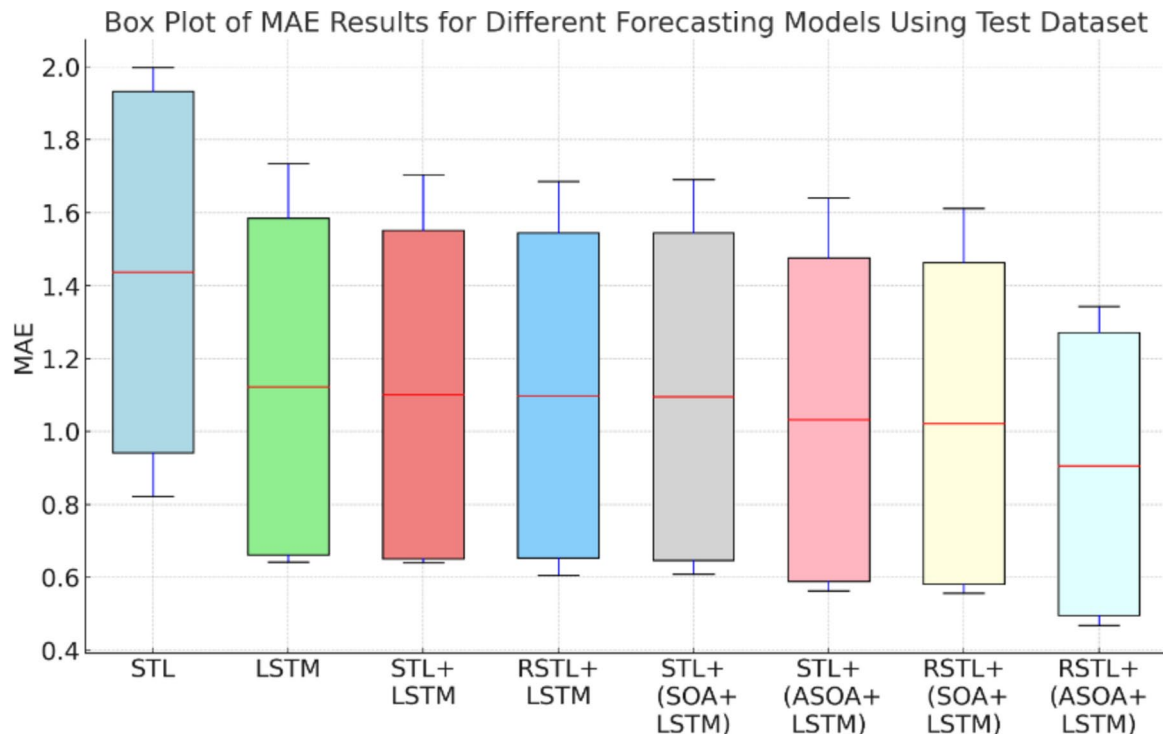


Fig. 13. MAE for testing dataset.

Predictor	Train Min	Train Max	Train Mean	Train STD	Val Min	Val Max	Val Mean	Val STD	Test Min	Test Max	Test Mean	Test STD
STL	0.609	1.803	1.198	0.472	0.734	1.926	1.312	0.486	0.823	1.998	1.437	0.495
LSTM	0.432	1.543	0.954	0.438	0.529	1.638	1.024	0.453	0.642	1.734	1.123	0.461
STL + LSTM	0.410	1.512	0.932	0.428	0.506	1.608	1.002	0.443	0.64	1.704	1.101	0.451
RSTL + LSTM	0.398	1.498	0.919	0.423	0.493	1.573	0.989	0.438	0.605	1.686	1.099	0.446
STL + (SOA + LSTM)	0.404	1.507	0.927	0.426	0.507	1.611	0.997	0.461	0.609	1.691	1.096	0.449
STL + (ASOA + LSTM)	0.392	1.492	0.914	0.421	0.488	1.587	0.936	0.426	0.563	1.641	1.033	0.444
RSTL + (SOA + LSTM)	0.386	1.485	0.907	0.418	0.482	1.55	0.903	0.413	0.557	1.612	1.022	0.441
RSTL + (ASOA + LSTM)	0.378	1.474	0.898	0.414	0.434	1.428	0.868	0.409	0.497	1.272	0.096	0.437

Table 6. MAE results for different prediction models.

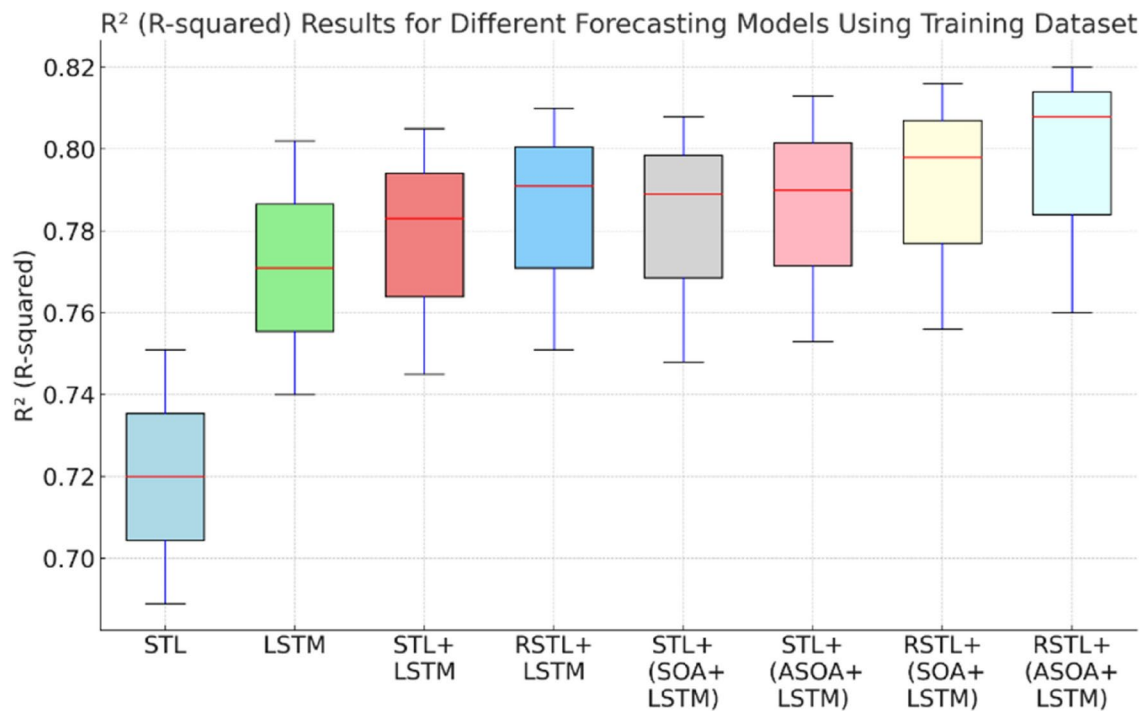
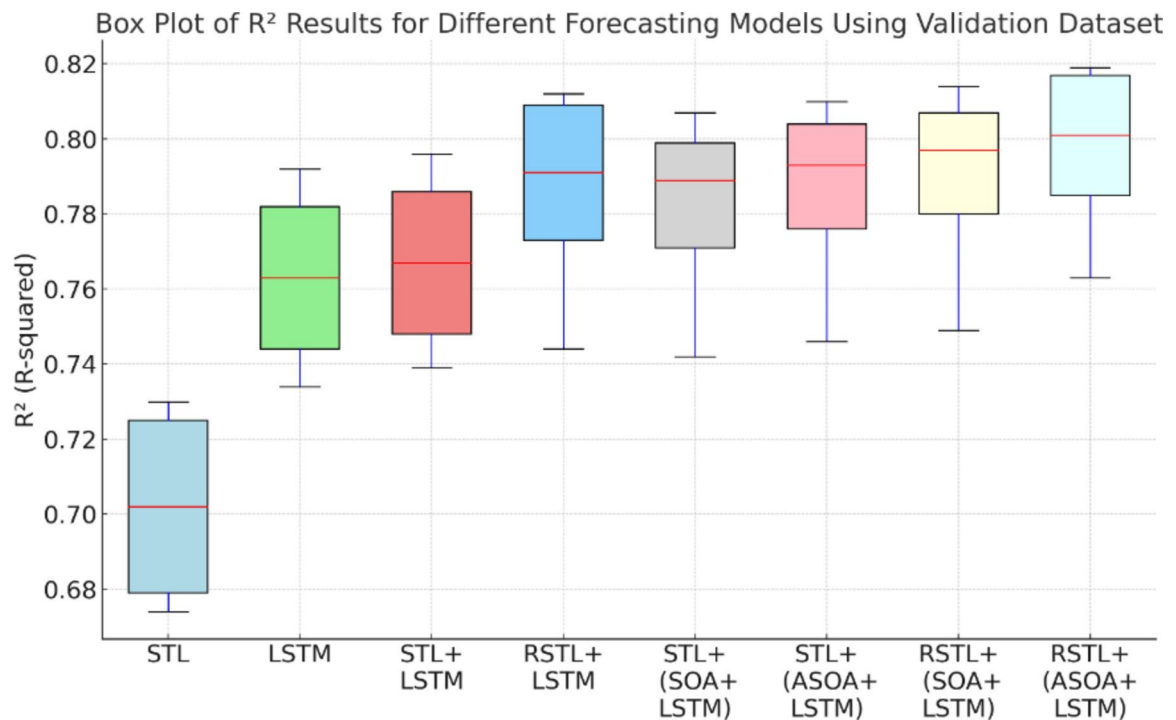
2. ASOA for dynamic optimization.

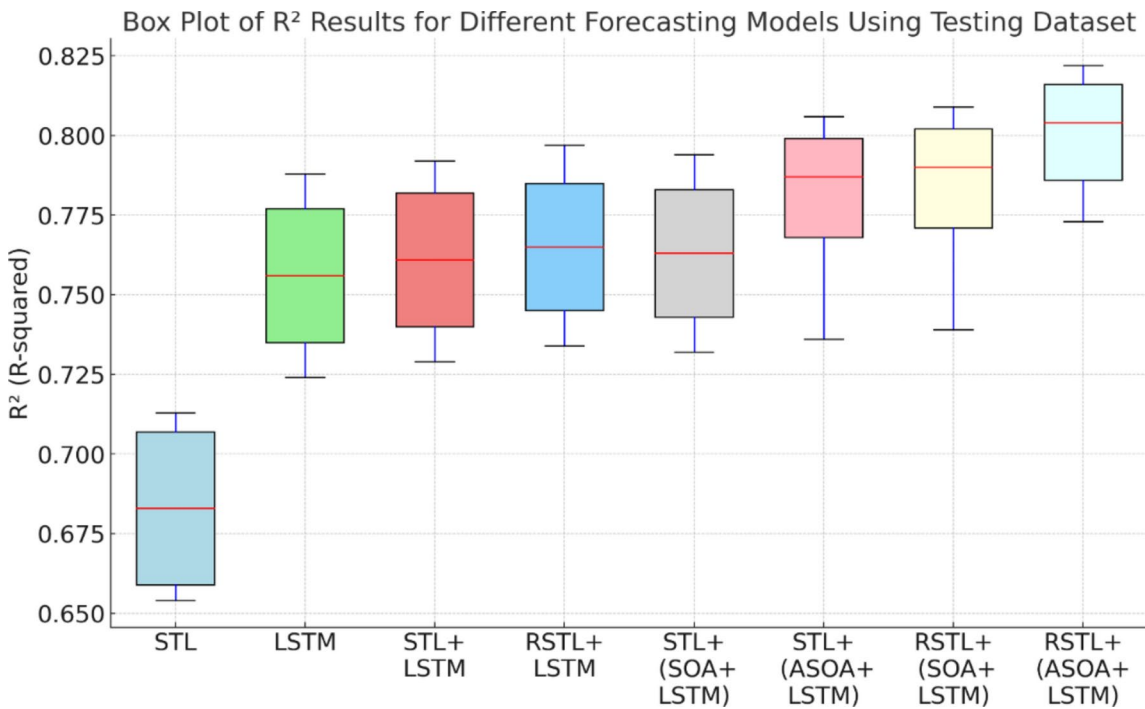
- Unlike static optimization methods, ASOA introduces a dynamic balance between exploration and exploitation, adapting the optimization process based on the current learning performance. This novel mechanism prevents premature convergence, a common issue in traditional optimization algorithms, and avoids getting trapped in local minima.
- By adjusting LSTM hyperparameters (such as gate weights and biases) during the training process, ASOA enhances the overall learning capability, enabling the model to adapt to complex data patterns more effectively.

Performance evaluation

The effectiveness of the proposed RSTL + (ASOA + LSTM) is demonstrated through performance metrics such as RMSE, MAE, and R^2 , which indicate substantial improvements in prediction accuracy when compared to baseline models:

1. *Reduction in RMSE* The proposed model achieves a 15.97% reduction in training RMSE, a 20.03% reduction in validation RMSE, and an 11.00% reduction in testing RMSE compared to the standard STL. This significant reduction highlights the improved capacity of the RSTL + ASOA to manage the variability in SE data.
2. *Improved MAE* The mean absolute error results highlight the model's superior performance. The proposed model reduces MAE by 25.04% in training, 33.84% in validation, and 39.58% in testing over the STL base-

**Fig. 14.** R² for training dataset.**Fig. 15.** R² for validation dataset.

**Fig. 16.** R^2 for training dataset.

Predictor	Train Min	Train Max	Train Mean	Train STD	Val Min	Val Max	Val Mean	Val STD	Test Min	Test Max	Test Mean	Test STD
STL	0.689	0.751	0.720	0.021	0.674	0.730	0.702	0.023	0.654	0.713	0.683	0.024
LSTM	0.740	0.802	0.771	0.020	0.734	0.792	0.763	0.019	0.724	0.788	0.756	0.021
STL + LSTM	0.745	0.805	0.783	0.020	0.739	0.796	0.767	0.019	0.729	0.792	0.761	0.021
RSTL + LSTM	0.751	0.810	0.791	0.019	0.744	0.812	0.791	0.018	0.734	0.797	0.765	0.020
STL + (SOA + LSTM)	0.748	0.808	0.789	0.019	0.742	0.799	0.789	0.018	0.732	0.794	0.763	0.020
STL + (ASOA + LSTM)	0.753	0.813	0.790	0.018	0.746	0.804	0.793	0.017	0.736	0.799	0.787	0.019
RSTL + (SOA + LSTM)	0.756	0.816	0.798	0.018	0.749	0.807	0.797	0.017	0.739	0.802	0.790	0.019
RSTL + (ASOA + LSTM)	0.760	0.820	0.808	0.017	0.763	0.819	0.801	0.016	0.773	0.816	0.804	0.018

Table 7. R^2 for different prediction models.

Metric	Value
Ljung-Box test p-value	0.015
PACF at Lag 1	0.58
PACF at Lag 2	0.45
PACF at Lag 3	0.31

Table 8. Performance results of PACF.

line. These reductions demonstrate the impact of AO and robust data decomposition on minimizing prediction errors.

3. *Enhanced R^2 values* With R^2 values of 0.808 for training, 0.801 for validation, and 0.804 for testing, the proposed model demonstrates a higher ability to capture the variability in data. These improvements in R^2 values—ranging from 12.22% to 17.71% compared to STL—indicate the model's more robust predictive capacity and overall accuracy.

Key contributions to predictive modeling

The combination of RSTL and ASOA + LSTM combines robust data decomposition and dynamic optimization. This improves the model's predictive accuracy and enhances its adaptability to highly volatile environments, such as those encountered in SE prediction. The model's ability to dynamically adjust its parameters based on

real-time learning allows it to refine predictions continuously, ensuring that the system remains responsive to new patterns and trends.

In summary, the novelty of the proposed model lies in its ability to address the inherent challenges in SE prediction—such as noise, seasonality, and complex data patterns—while significantly improving predictive accuracy through AO and robust decomposition. This positions the RSTL+(ASOA+LSTM) as an advanced solution in RE prediction, with potentially real-world applications in grid management and energy optimization.

Conclusion and future work

By integrating RSTL with an ASOA-optimized LSTM-neural network, this paper presented an inventive model for PV-SE prediction. With the effective use of RSTL, noises are addressed, and there were rapid changes and outliers in time series data, leading to an abrupt and more robust foundation for accurate prediction. During the optimization process, the seagull's migratory and foraging behaviours, dynamically balanced exploration, and exploitation inspired ASOA, thus improving the LSTM's performance. Historical SE data and relevant meteorological parameters based on experimental evaluation revealed that the proposed RSTL+(ASOA+LSTM) persistently outdid many baseline models, such as solo STL, LSTM, and their respective optimization techniques. The proposed model significantly improved prediction accuracy, measured by RMSE, MAE, and R^2 performance measures. These findings highlight the benefits of integrating robust data decomposition techniques with AO algorithms for dealing with the complexities and oscillations inherent in SE data. The proposed approach improves prediction accuracy and provides a scalable and reliable setup for SE management.

Future research can emphasize refining the optimization algorithm, incorporating it with other *state-of-the-art* ML techniques, and applying it to numerous Renewable Energy Sources. This work faces practical implications since it proposes a robust tool for enhancing the SE model's efficiency and dependability, finally contributing to the larger goal of RE solutions.

Data availability

The datasets used and/or analysed during the current study available from the corresponding author on reasonable request.

Received: 22 August 2024; Accepted: 21 January 2025

Published online: 03 February 2025

References

- Hasan, M. M. et al. Harnessing solar power: A review of photovoltaic innovations, solar thermal systems, and the dawn of energy storage solutions. *Energies* **16**(18), 6456 (2023).
- Simankov, V. S., Buchatskiy, P. Y., Onishchenko, S. V. & Teplovkhov, S. V. Review of models for estimating and predicting the amount of energy produced by solar energy systems. *Russ. J. Earth Sci.* **5**, 1–17 (2023).
- Cui, L. & Liao, J. Intelligent power grid energy supply forecasting and economic operation management using the snake optimizer algorithm with Bigur-attention model. *Front. Energy Res.* **11**, 1273947 (2023).
- Sammar, M. J. et al. Illuminating the future: A comprehensive review of AI-based solar irradiance prediction models. *IEEE Access*.
- Martínez-Soto, L. F., Rodríguez-Zalapa, O., López-Fernández, J. A., Castellanos-Galindo, J. J., & Tovar-Hernández, J. H. Evaluation of univariate time-series models for short-term solar energy forecasting. In *Congress on Research, Development and Innovation in Renewable Energies: Selected Papers from CIDiER 2021*, 13–32. (Springer, 2022).
- Chaudhary, S. *Forecasting of Solar Electricity Generation and Performance Evaluation of Forecasting Models Using Time Series Data*. Doctoral dissertation, Dublin, National College of Ireland. (2017).
- Kalogiriou, S. A. *Solar Energy Engineering: Processes and Systems* (Elsevier, 2023).
- Allal, Z., Noura, H. N., Salman, O. & Chahine, K. Machine learning solutions for renewable energy systems: Applications, challenges, limitations, and future directions. *J. Environ. Manag.* **354**, 120392 (2024).
- Zameer, A. et al. Short-term solar energy forecasting: Integrated computational intelligence of LSTMs and GRU. *PLoS ONE* **18**(10), e0285410 (2023).
- Li, D., Jiang, M. R., Li, M. W., Hong, W. C. & Xu, R. Z. A floating offshore platform motion forecasting approach based on EEMD hybrid ConvLSTM and chaotic quantum ALO. *Appl. Soft Comput.* **144**, 110487 (2023).
- Cornaro, C., Pierro, M. & Bucci, F. Master optimization process based on neural networks ensemble for 24-h solar irradiance forecast. *Sol. Energy* **111**, 297–312 (2015).
- Sbrana, G. & Silvestrini, A. Random switching exponential smoothing and inventory forecasting. *Int. J. Prod. Econ.* **156**, 283–294 (2014).
- Ferbar Tratar, L. & Strmcnik, E. The comparison of Holt-Winters method and Multiple regression method: A case study. *Energy* **109**, 266–276 (2016).
- Mora-Lopez, L. & Sidrach-de-Cardona, M. Multiplicative ARMA models to generate hourly series of global irradiation. *Sol. Energy* **63**(5), 283–291 (1998).
- Hansen, B. E. *Time Series Analysis James D* Vol. 11, 625–630 (Hamilton Princeton University Press, 1994).
- Reikard, G. Predicting solar radiation at high resolutions: A comparison of time series forecasts. *Sol. Energy* **83**(3), 342–349 (2009).
- AlKandari, M. & Ahmad, I. Solar power generation forecasting using ensemble approach based on deep learning and statistical methods. *Appl. Comput. Inform.* **20**(3/4), 231–250 (2024).
- Haider, S. A., Sajid, M., Sajid, H., Uddin, E. & Ayaz, Y. Deep learning and statistical methods for short-and long-term solar irradiance forecasting for Islamabad. *Renew. Energy* **198**, 51–60 (2022).
- Elsaraiti, M. & Merabet, A. Solar power forecasting using deep learning techniques. *IEEE Access* **10**, 31692–31698 (2022).
- Liu, C. H., Gu, J. C. & Yang, M. T. A simplified LSTM neural network for one day-ahead solar power forecasting. *IEEE Access* **9**, 17174–17195 (2021).
- Gundu, V. & Simon, S. P. Short-term solar power and temperature forecast using recurrent neural networks. *Neural Process. Lett.* **53**(6), 4407–4418 (2021).
- Beigi, M. et al. Forecasting of power output of a PVPS based on meteorological data using RNN approaches. *Sustainability* **14**(5), 3104 (2022).
- Vijay, V., Kumar, R., Sharma, A. & Kumar, A. Short-term forecasting of Solar Irradiance using STL, Wavelet, and LSTM. *Int. J. Comput. Appl.* **183**(46), 9–17 (2022).

24. Kumar, S. S., & Sam, K. N. Multi-hybrid STL-LSTM-SDE-MA model optimized with IWOA for solar PV-power forecasting. In *2023 IEEE International Conference on Power Electronics, Smart Grid, and Renewable Energy (PESGRE)*, 1–6. (IEEE, 2023).
25. Wen, Q., Gao, J., Song, X., Sun, L., Xu, H., & Zhu, S. RobustSTL: A robust seasonal-trend decomposition algorithm for long-time series. In *Proceedings of the AAAI Conference on Artificial Intelligence*, Vol. 33, No. 01, 5409–5416 (2019).
26. Dhiman, G. & Kumar, V. Seagull optimization algorithm: Theory and its applications for large-scale industrial engineering problems. *Knowl. Based Syst.* **165**, 169–196 (2019).
27. Khan, G. et al. Energy-efficient routing algorithm for optimizing network performance in underwater data transmission using gray wolf optimization algorithm. *J. Sens.* **2024**, 2288527. <https://doi.org/10.1155/2024/2288527> (2024).
28. Vinothini, A. et al. An artificial-intelligence-based renewable energy prediction program for demand-side management in smart grids. *Sustainability* **15**(6), 5453. <https://doi.org/10.3390/su15065453> (2023).
29. Abdulkader, R. et al. Soft computing in smart grid with decentralized generation and renewable energy storage system planning. *Energies* **16**(6), 2655. <https://doi.org/10.3390/en16062655> (2023).
30. Karn, A. L. et al. An empirical analysis of the effects of energy price shocks for sustainable energy on the macro-economy of south Asian countries. *Energies* **16**(1), 363. <https://doi.org/10.3390/en16010363> (2023).
31. Rajagopalan, A. et al. Modernized planning of smart grid based on distributed power generations and energy storage systems using soft computing methods. *Energies* **15**(23), 8889. <https://doi.org/10.3390/en15238889> (2022).
32. Singh, N. P. et al. Investigation on characteristics of Monte Carlo model of single electron transistor using Orthodox Theory. *Sustain. Energy Technol. Assess.* **48**, 101601. <https://doi.org/10.1016/j.seta.2021.101601> (2021).
33. Neffati, O. S. et al. Migrating from traditional grid to smart grid in smart cities promoted in developing country. *Sustain. Energy Technol. Assess.* **45**, 101125. <https://doi.org/10.1016/j.seta.2021.101125> (2021).
34. Sathish Kumar, K. et al. Area-based efficient and flexible demand side management to reduce power and energy using evolutionary algorithms. *Malay. J. Comput. Sci.* **2020**, 27335 (2020).
35. Yang, M., Jiang, Y., Zhang, W., Li, Y. & Su, X. Short-term interval prediction strategy of photovoltaic power based on meteorological reconstruction with spatiotemporal correlation and multi-factor interval constraints. *Renew. Energy* **237**, 121834. <https://doi.org/10.1016/j.renene.2024.121834> (2024).
36. Yang, M., Che, R., Yu, X. & Su, X. Dual NWP wind speed correction based on trend fusion and fluctuation clustering and its application in short-term wind power prediction. *Energy* **302**, 131802. <https://doi.org/10.1016/j.energy.2024.131802> (2024).
37. Li, N., Dong, J., Liu, L., Li, H. & Yan, J. A novel EMD and causal convolutional network integrated with Transformer for ultra short-term wind power forecasting. *Int. J. Electr. Power Energy Syst.* **154**, 109470. <https://doi.org/10.1016/j.ijepes.2023.109470> (2023).
38. Sun, K. et al. Output power prediction of stratospheric airship solar array based on surrogate model under global wind field. *Chin. J. Aeron.* <https://doi.org/10.1016/j.cja.2024.09.020> (2024).
39. Meng, Q. et al. Enhancing distribution system stability and efficiency through multi-power supply startup optimization for new energy integration. *IET Gener. Transm. Distrib.* **18**(21), 3487–3500. <https://doi.org/10.1049/gtd2.13299> (2024).
40. Zhang, C., Zeng, Q., Dui, H., Chen, R. & Wang, S. Reliability model and maintenance cost optimization of wind-photovoltaic hybrid power systems. *Reliab. Eng. Syst. Saf.* **255**, 110673. <https://doi.org/10.1016/j.ress.2024.110673> (2025).

Author contributions

Conceptualization, Methodology, Software, Validation, Formal analysis, Investigation, Resources, Data Curation, Writing—Original Draft, Writing—Review & Editing, Visualization : Venkatachalam Mohanasundaram and Balamurugan Rangaswamy.

Declarations

Competing interests

The authors declare no competing interests.

Additional information

Correspondence and requests for materials should be addressed to V.M.

Reprints and permissions information is available at www.nature.com/reprints.

Publisher's note Springer Nature remains neutral with regard to jurisdictional claims in published maps and institutional affiliations.

Open Access This article is licensed under a Creative Commons Attribution-NonCommercial-NoDerivatives 4.0 International License, which permits any non-commercial use, sharing, distribution and reproduction in any medium or format, as long as you give appropriate credit to the original author(s) and the source, provide a link to the Creative Commons licence, and indicate if you modified the licensed material. You do not have permission under this licence to share adapted material derived from this article or parts of it. The images or other third party material in this article are included in the article's Creative Commons licence, unless indicated otherwise in a credit line to the material. If material is not included in the article's Creative Commons licence and your intended use is not permitted by statutory regulation or exceeds the permitted use, you will need to obtain permission directly from the copyright holder. To view a copy of this licence, visit <http://creativecommons.org/licenses/by-nc-nd/4.0/>.

© The Author(s) 2025